

	001
	002
	003
	004
	005
	006
	007
Brain Dynamics	008
	009
	010
	011
Alexander Mark Weber <sup>1,2*</sup>	012
	013
	014
<sup>1</sup> BC Children's Hospital Research Institute, The University of British Columbia, 938 West 28th Avenue, Vancouver, V5Z 4H4, Canada.	015
	016
	017
<sup>2</sup> Pediatrics, The University of British Columbia, 2329 West Mall, Vancouver, V6T 1Z4, Canada.	018
	019
	020
	021
	022
Corresponding author(s). E-mail(s): <a href="mailto:aweber@bcchr.ca">aweber@bcchr.ca</a> ;	023
	024
	025
	026
<b>Abstract</b>	027
An introduction to the idea of brain dynamics in fMRI studies	028
	029
	030
	031
	032
<sup>1</sup> The University of British Columbia	033
	034
<sup>2</sup> The University of British Columbia	035
	036
* Correspondence: Alexander Mark Weber < <a href="mailto:aweber@bcchr.ca">aweber@bcchr.ca</a> >	037
	038
	039
	040
	041
	042
A fractal structure, either spatial or temporal, is composed of smaller parts that exhibit the same pattern at every scale [1–3]. Classic spatial examples of fractals in nature	043
	044
	045
	046

047 are coastlines [3], circulatory system [4], and brain anatomy [5], where at each level of  
048 magnification these structures look the same; i.e. *self-similarity*. For a dynamic process,  
049 or in the temporal domain, this is known as *scale invariance*, meaning that both rapid  
050 and slow processes follow the same pattern [6]. Scale-free behavior, characterized by  
051 the absence of any inherent scale or preferred length, is a signature characteristic  
052 of complex systems that can be understood as the collective outcome of numerous  
053 interacting components with weak and random connections [7]. Physiological systems  
054 usually need a mix of randomness and structure to function optimally. When a system  
055 is operating near the critical point, it is expected to exhibit these long range temporal  
056 correlations (LRTCs). Therefore, by analyzing the LRTC of a time-series, valuable  
057 insights can be found into the underlying mechanisms driving system behavior, such  
058 as memory effects, self-organization, and criticality [8].  
059  
060

---

061  
062  
063  
064  
065  
066  
067  
068  
069  
070  
071 “Because pink noise lies between white and Brown(ian) noise, it has been proven  
072 to bring stability and adaptability into dynamic processes, thus, crucial properties of  
073 well-functioning complex systems” [9]  
074  
075  
076  
077 “as pink noise arises from the interaction of multiple systems and operates over different  
078 scales, it has been shown to contribute to system resiliency and structural integrity if  
079 individual components were lost or interrupted” [10, 11]  
080  
081

082 See Herman et al. [12] for a really good review  
083  
084

085 Scale-free dynamics is a hallmark of complexity viewed as an emergent property of biolog-  
086 ical systems composed of numerous elements with a network of stochastic (typically weak)  
087 connections amongst them (Csermely, 2006) from Mukli et al. [13]  
088  
089

090  
091  
092

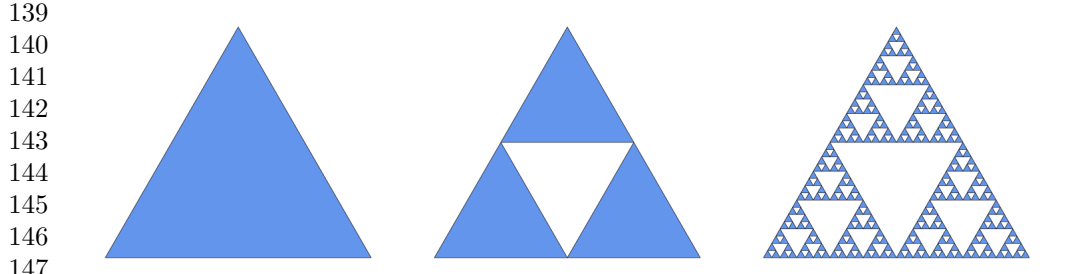
Another good review is by Werner (2010) linking fractals/Hurst and Criticality Werner [14]	093
	094
	095
	096
	097
	098
	099

---

## Fractal Dimension and Hurst Exponent

Non-periodic fluctuations are prevalent in physiological systems, and these irregular patterns can be mathematically modeled using stochastic, chaotic, or noisy chaotic methods. Stochastic models assume that the fluctuations result from a large number of weak influences, while chaotic models conceptualize that strong nonlinear interactions between a few factors shape the fluctuations. Among the various stochastic approaches, ‘fractal’ models offer the most accurate representation of reality by considering the self-similar nature of physiological fluctuations over different time scales [15]. Fractal structures were first expressed in the late 19th and early 20th century by mathematicians who generated complex geometrical structures with simple objects (e.g. a triangle) by applying a simple rule of transformation in an infinite number of iterative steps Figure 1. A use-case for these geometric structures was not fully realized until the 1960s, when Benoit Mandelbrot formalized them as a new form of geometry capable of describing the complex shapes and forms of nature [3].

	100
	101
	102
	103
	104
	105
	106
	107
	108
	109
	110
	111
	112
	113
	114
	115
	116
	117
	118
	119
	120
	121
	122
	123
	124
	125
	126
	127
	128
	129
	130
	131
	132
	133
	134
	135
	136
	137
	138



139  
140  
141  
142  
143  
144  
145  
146  
147  
148 **Figure 1. Ideal mathematical fractal.** The 2D Sierpinski triangle starts with a  
149 simple equilateral triangle (left), and subdivides it recursively into smaller equilateral  
150 triangles. For every iteration, each triangle (in blue) is further subdivided it into four  
151 smaller congruent equilateral triangles with the central triangle removed. The first  
152 such iteration is shown in the centre, with the fifth iteration shown on the right.  
153  
154  
155  
156

157 Unlike Euclidean structures that can use axioms and rules to describe an object of  
158 integer dimensions, fractal structures can only be characterized by recursive algo-  
159 rithms that extend the use of dimension to the non-integer range [16]. Recognizing this  
160 difference, Mandelbrot named these complex structures ‘fractals’, and defined their  
161 non-Euclidean dimension as a ‘fractal dimension’ (FD) — that is, a non-integer. For  
162 the one-dimensional time-series, FD will be between 1 and 2. While a structure such  
163 as the Sierpinski triangle is an ‘exact fractal’, meaning it is assembled from pieces  
164 that are an exact replica of the whole, nature is composed of ‘statistical fractals’,  
165 whose self-similarity is found in the power law scaling of the parameters characterizing  
166 their structures at different scales of observation Figure 2. Unlike Euclidean struc-  
167 tures which can be defined by axioms, fractals can only be characterized by a set of  
168 properties that, when present, indicate the structure is indeed fractal (see Section 2).  
169  
170  
171  
172  
173  
174  
175  
176  
177  
178 The Hurst exponent ( $H$ ) is a statistical measure used to quantify long-range depen-  
179 dence or persistence in time-series data (i.e. LRTCs). First introduced by Harold Hurst  
180 in 1951 for hydrological applications [18], it was Mandelbrot again who helped pop-  
181 ularize its use for studying complex shapes and forms of nature [3, 19]. Since then  
182  
183  
184

185  
186  
187  
188  
189  
190  
191  
192  
193  
194  
195  
196  
197  
198  
199  
200  
201  
202  
203  
204  
205  
206  
207  
208  
209  
210  
211  
212  
213  
214  
215  
216  
217  
218  
219  
220  
221  
222  
223  
224  
225  
226  
227  
228  
229  
230

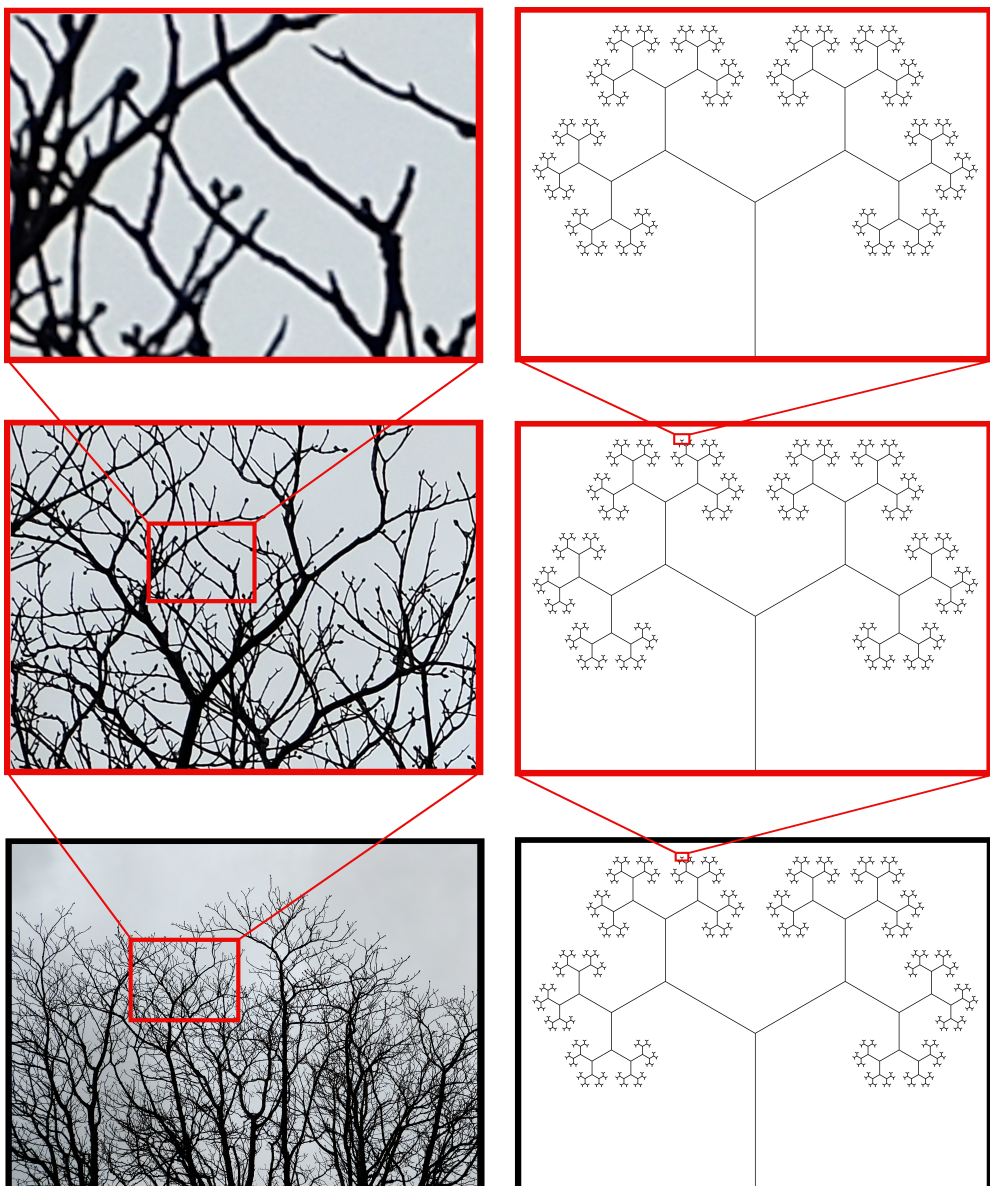


**Figure 2. A comparison of statistical and exact fractal patterns.** The two basic forms of fractals are demonstrated. Zooming in on tree branches (left), an exact self-similar element cannot be found. Zooming in on an exact fractal (right), exact replica of the whole are found. Photo by author. Branching fractal made in Python. Figure inspired by Taylor (2006) [17]

231 it has been applied across various fields, including finance, geophysics, ecology, and  
232 neuroscience, to characterize complex systems with intricate dynamics [20–23]. H and  
233 FD for time-series can be directly converted, as

235

236

237

238

$$H = 2 - D. \quad (1)$$

239

240

241 This means that FD and H are inversely correlated, and that H is a real number  
242 between 0 and 1 (non-inclusive; although it can be extended to  $> 1$ ; see ...). For the  
243 rest of this paper, we will be discussing H.

244

245

246 *Thus, the basic premise behind fractal time-series analysis is that, beneath the seem-*  
247 *ingly chaotic and unpredictable variations in the signal, there lies a stable underlying*  
248 *mechanism which can be effectively described using the fewest possible parameters*  
249 *(i.e. H or FD).*

250

251

252

## Properties

253

254

255 When  $H = 0.5$  ( $FD = 1.5$ ), the time-series is completely uncorrelated, has no memory,  
256 and is like white noise (pure random). It represents the highest level of unpredictability  
257 and entropy, but not necessarily the most complex state in a physiological sense. When  
258  $H < 0.5$  ( $FD > 1.5$ ), the time-series is said to be anti-persistent, exhibiting negative  
259 correlations: i.e. if the signal increases at one point, it's likely to decrease at the next  
260 point. This is also known as short-term reversal. This tends to make the time-series  
261 more predictable and reduces randomness, often simplifying dynamics. When  $H >$   
262  $0.5$  ( $FD < 1.5$ ), the time-series exhibits positive long-range correlations, and is more  
263 structured. The time-series displays a long-term trend, meaning past states influence  
264 future states.

265

266

267

268

269

270

271

272

There are four main properties that must be present for a time-series to be characterized by H or FD: 1) self-similarity; 2) power law scaling relationship; 3) scale-invariance; and 4) a scaling range (**?@fig-fourprop**). Each of these will be discussed in turn.

## Self-similarity

Self-similarity means that pieces of the structure, when enlarged, resemble larger pieces or the whole (Figure 2 and **?@fig-fourprop A-C**). Technically speaking, physiological time-series are self-affine, meaning their scaling is anisotropic (i.e. the proportions between enlarged pieces are different in one direction from those in the other). This is because in one direction (time) the proportions between the enlarged pieces is different than in the other (amplitude of signal; e.g. fMRI BOLD) [24].

## Power law scaling relationship

Power law scaling means that, for a quantitative property,  $q$ , is measured in quantities of  $s$ , its value depends on  $s$  according to the following scaling relationship:

$$q = f(s). \quad (2)$$

For non-fractal objects, the estimate of  $q$  using progressively smaller units of measure  $s$  will converge to a single value as the size of the measurement units approaches zero. On the other hand, fractals exhibit a power law scaling relationship with  $s$ , whereby the estimated value of  $q$  increases without limit as the size of the  $s$  decreases.

$$q = ps^\epsilon \quad (3)$$

323 where  $p$  is a factor of proportionality (prefactor) and  $\epsilon$  is a negative number, the  
 324 scaling exponent. The value of  $\epsilon$  can be determined as the slope of the linear regression  
 325 fit to the data pairs on the plot of  $\log q$  versus  $\log s$ :  
 326

$$\log q = \log p + \epsilon \log s \quad (4)$$

333 Data points for exact fractals will line up along perfectly with regression slope, while  
334 statistical fractals scatter around it since the two sides of Equation 4 are equal only  
335 in distribution.

## Scale-invariance

The ratio of two estimates of  $q$  measured at two different scales,  $s_1$  and  $s_2$ ,  $q_2/q_1$  depends only on the ratio of scales (relative scale),  $s_2/s_1$ , and not directly on the absolute scale,  $s_1$  or  $s_2$

$$q_2/q_1 = ps_2^\epsilon / ps_1^\epsilon = (s_2/s_1)^\epsilon \quad (5)$$

For statistical fractals, like those of nature,  $s_2/s_1$  may change in a continuous fashion still leaving the validity of Equation 5 unaffected. The scale-invariance of fractals arises from the fact that the geometrical structure only depends on the scaling factor (ratio of scales), and not the absolute scale. As a result, quantitative properties of smaller parts are similar to those of larger parts.

## Scaling range

Natural fractals may only display scale-invariance within a restricted range, as they are finite (either by definition or due to the fact that they must be sampled). The upper cut-off point ( $s_{max}$ ) in Equation 6, falls within the size range of the structure itself.

Similarly, the lower cut-off point ( $s_{min}$ ) falls within the dimensions of the smallest structural elements. The scaling range (SR) is defined in decades

$$SR = \log_{10}(s_{max}/s_{min}) \quad (6)$$

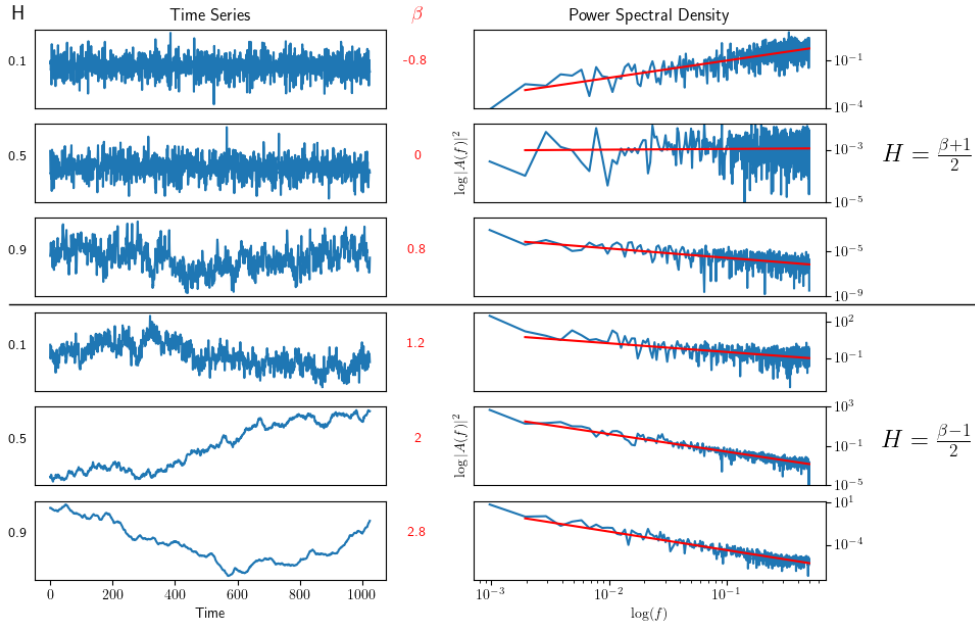


**Figure 3. Simulated fractional Gaussian noise and fractional Brownian motion.** Raw simulated time-series with 1,024 time-points and known Hurst values. Signals were created using the Davies-Harte method. a-c) are fractional Gaussian noise while d-f are fractional Brownian motion. a) and d) have H values of 0.1; b) and e) have H values of 0.5; and c) and f) have H values of 0.9. Note how fractional Gaussian noise remain centered around a mean (i.e. stationary), while fractional Brownian motion is free to wander (i.e. non-stationary). Exact fractal time-series were created using the Davies-Harte method.

If the class of signal is not appropriately identified — for example, when  $\beta$  is  $\sim 1$  — it is possible to seriously miscalculate the H value, such that a true  $H \sim 0.9$  will be

415 calculated as 0.1. Therefore, algorithms and research in properly classifying fractal  
416 signals is crucially important.  
417

418

419 **Prerequisites to measuring H**

420

421 **Time-points**

422

423 Before determining if a time-series exhibits a power-law scaling relationship, one  
424 should first determine if the time-series has enough time-points to do so. The rule  
425 of thumb is that the power law relationship should be present in a range larger  
426 than two decades in the frequency domain of a PSD [24]. Due to the Whittaker–  
427 Nyquist-Shannon sampling theorem [25], one requires two times as many time-points  
428 as frequency samples. Since two decades in the frequency domain is 100 distinct  
429 frequencies, one would required at least 200 time-points to proceed.  
430

431

432

433 **Power-law scaling relationship**

434

435 The next step would be to perform a periodogram or PSD and test for a power-law  
436 scaling relationship. Usually power laws are tested using a probability distribution  
437 [26]. However, as the PSD is not a probability distribution, alternative methods must  
438 be used. A goodness-of-fit test can be devised based on Clauset et al. [26], which can  
439 also help us derive the SR (i.e.  $freq_{min}$  and  $freq_{max}$ ). First, a PSD is produced, and  
440 the variance ( $\sigma^2$ ),  $\beta$ , and H are computed using Equation 8. Next, the Kolmogorov–  
441 Smirnov statistic [27, 28] is used to measure the distance D between the raw PSD data-  
442 points and the best-fit linear-regression line used to calculate H (i.e. the residuals).  
443 The D in this case is the largest residual error. Then, 1,000 time series of either fGn  
444 or fBm (depending on what value of  $\beta$  was found; see Equation 8) with the same  
445 length ( $n > 200$ ),  $\sigma^2$ , and Hurst exponent are generated using one of several methods  
446 for producing exact fractal signals: spectral synthesis method (SSM) [29], Davies–  
447 Harte method (DH) [30], Cholesky method [31], or the Hosking’s method [32]. Each  
448

449

450

451

452

453

454

455

456

457

458

459

460

synthetic time-series is converted to a PSD, and the Kolmogorov–Smirnov statistic	461
is used to measure the distance D between the raw PSD data-points and the best-fit	462
linear-regression line. The $p$ -value is defined as the fraction of synthetic time series	463
with Ds that are larger than the original D of the original time-series. The larger the	464
$p$ -value, the more plausible the synthetic model (either fGn or fBm) is for representing	465
the original time-series, and the better the fit of the original data to a scale-free	466
distribution. The null-hypothesis that the time-series is not scale free is rejected if $p$	467
< 0.05 (i.e. if $p > 0.05$ , we say that the time-series is scale-free).	468
	469
	470
	471
	472
	473
	474
However, this method can be computationally intensive, and prone to false negatives,	475
especially signals with very high or low H values. One solution is, instead of applying	476
this test to every voxel in a 4D fMRI brain scan, to segment the brain into separate	477
ROIs (e.g. anatomically based on an atlas, or functionally by first running ICA to	478
identify RSNs), average the time-series within each ROI, which will improve SNR,	479
and then run the power-law scaling test.	480
	481
	482
	483
	484
	485
A sample python code is provide in Section 2	486
	487
	488
<b>Scaling range</b>	489
<b>fGn or fBm</b>	490
<b>Choosing the right method</b>	491
Ideally therefore, a long memory process signal should be categorized as either stationary	492
(fGn) or non-stationary (fBm) and the variance and correlation defined. from [24]	493
	494
	495
	496
	497
	498
	499
<b>Methods of measuring H</b>	500
Fractal methods are diverse, but their approaches have one thing in common in that	501
they employ equation (2) in fitting their proposed model to data pairs of log feature	502
versus log scale for finding the scaling exponent, , from the regression slope. Each fractal	503
	504
	505
	506

507 analysis tool has different performance, prerequisite conditions, and limitations, and each  
508 needs thorough evaluation in order to avoid bias or misinterpretation of the derived fractal  
509 parameters [5, 6, 8, 9], especially when applied to physiological signals which may be  
510 contaminated with noise [15, 28]. from [24]  
511

512

513

514

## 515 Neuroscience Applications

516

517 H has emerged as a valuable tool in neuroscience and clinical research. Typically, H  
518 values reported in adult brains are above 0.5, with higher H values in grey matter  
519 than white matter or cerebrospinal fluid [33, 34]. Some key findings from neuroscience  
520 research include: a decrease in H during task performance [35, 36]; negative corre-  
521 lations with task novelty and difficulty [37]; increases with age in the frontal and  
522 parietal lobes [33], and hippocampus [38]; decreases with age in the insula, and lim-  
523 bic, occipital and temporal lobes [33]; H < 0.5 in preterm infants [39]; and more [40].  
524 In terms of clinical findings, abnormal H values have been identified in Alzheimer's  
525 disease (AD) [41, 42], autism spectrum disorder (ASD) [43–46], mild traumatic brain  
526 injury [47], major depressive disorder [48, 49] and schizophrenia [46, 50].  
527

528

529

## 530 fMRI preprocessing considerations

531

532

### 533 Nuisance regression

534

535

536 When attempting to regress out non-BOLD signal, it is important to apply the regres-  
537 sion at the same time, and not in succession. Even performing a band-pass filter after  
538 nuisance regression can re-introduce noise components [51].  
539

540

541

542

### 543 Detrending

544

545

546

547 see Tanabe et al. [52]

548

549

550

551

552

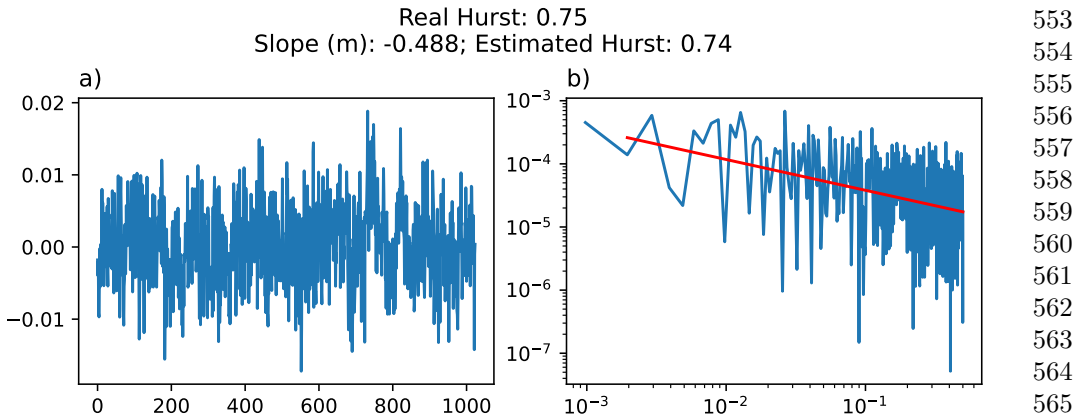


**Figure 4. Simulated fractional Gaussian noise.** a) Raw simulated time-series with 1,024 time-points and a known Hurst value of 0.75; b) The same signal from a) in a log-log power spectral density plot and a linear-regression used to calculate the estimated Hurst value.

## Hurst Reviews

Nonparametric trend estimation in the presence of fractal noise:

Application to fMRI time-series analysis - Afshinpour et al. (2008)

[53]

In this paper, a method for estimating trend in the presence of fractal noise is proposed and applied to fMRI time-series. To this end, a partly linear model (PLM) is fitted to each time-series. The parametric and nonparametric parts of PLM are considered as contributions of hemodynamic response and trend, respectively. Using the whitening property of wavelet transform, the unknown components of the model are estimated in the wavelet domain. The results of the proposed method are compared to those of other parametric trend-removal approaches such as spline and polynomial models. It is shown that the proposed method improves activation detection and decreases variance of the estimated parameters relative to the other methods.

Notes:

- trend estimation paper
  - 1.5T, 3.9x3.9x6mm, 1.648s TR, 256 time-points
  - Hurst method: Wavelet db4 with 5 scales

## 605 Fractal Analysis of BOLD time-series in a Network Associated With 606

607 Waiting Impulsivity - Akhrif et al. (2018) [54]  
608

examined **103** healthy male students at **rest** and while performing the 5-choice serial reaction time **task**. We addressed fractality in a network associated with waiting impulsivity using the **adaptive fractal analysis (AFA)** approach to determine H. We revealed the fractal nature of the impulsivity network. Furthermore, fractality was influenced by individual impulsivity in terms of decreasing fractality (H) with higher impulsivity in regions of top-down control (left middle frontal gyrus) as well as reward processing (nucleus accumbens and anterior cingulate cortex).

621 Notes:

- fMRI split into low and high frequency components. LFC is the second order polynomial that is a smooth and global fit of the original time course.
  - AFA: variance of fluctuation computed around, in this case, a second order polynomial trend  $v(i)$  fitted to time-series within each segment  $w$ , and its size:

$$F(w) = \sqrt{\frac{1}{N} \sum_{i=1}^N (u(i) - v(i))^2} \sim w^H \quad (7)$$

636 *N*: length of the time-series

$$w = 2n + 1, n = 5, 6, \dots, 13$$

<sup>643</sup> H is determined as the slope of the log-log plot  $\log_2(F(w))$  as a function of  $\log_2(w)$

```

Example code:                                645
                                                646
import numpy as np                         647
                                            648
                                            649
def adaptive_fractal_analysis(signal, n_values=range(5, 14)): 650
    """                                         651
                                                652
                                                653
                                                Perform Adaptive Fractal Analysis (AFA) to compute the Hurst exponent. 654
                                                655
                                                656
Parameters:                                 657
                                                658
                                                659
    signal (array-like): time-series data to analyze.           660
    n_values (iterable): Sequence of `n` values to define window sizes as w = 2n + 1. 661
                                                662
                                                663
Returns:                                    664
                                                665
                                                666
    float: Estimated Hurst exponent (H).                      667
    """
                                                668
# Define window sizes as w = 2n + 1          669
window_sizes = [2 * n + 1 for n in n_values] 670
fluctuations = []                            671
                                                672
                                                673
                                                674
for window_size in window_sizes:            675
    segment_variances = []                  676
    for start in range(0, len(signal) - window_size + 1, window_size): 677
        # Extract the window                678
        window = signal[start:start + window_size] 679
        # Fit a second-order polynomial (quadratic fit) and compute residual 680
        x = np.arange(len(window))           681
        p = np.polyfit(x, window, deg=2)    # Degree 2 polynomial       682
        residual = window - np.polyval(p, x) 683
                                                684
                                                685
                                                686
                                                687
                                                688
                                                689
                                                690

```

```

691     # Compute variance of the residuals
692     variance = np.var(residual)
693     segment_variances.append(variance)
694
695
696
697     # Compute average variance for this window size
698     fluctuations.append(np.mean(segment_variances))
699
700
701
702     # Fit the scaling law: log(fluctuations) vs. log(window_sizes)
703     log_window_sizes = np.log(window_sizes)
704     log_fluctuations = np.log(fluctuations)
705
706     slope, intercept = np.polyfit(log_window_sizes, log_fluctuations, deg=1)
707
708
709
710     # The slope corresponds to the Hurst exponent
711
712     return slope
713
714
715
716 Endogenous human brain dynamics recover slowly following
717
718 cognitive effort - Barnes et al. (2009) [55]
719
720 1) Does performance of a cognitively effortful task significantly change fractal
721 scaling properties of fMRI time-series compared to their values before task per-
722 formance? 2) If so, can we relate the extent of task-related perturbation to the
723 difficulty of the task? This result supports the model that endogenous low fre-
724 quency oscillatory dynamics are relevant to the brain's response to exogenous
725 stimulation. Moreover, it suggests that large-scale neurocognitive systems mea-
726 sured using fMRI, like the heart and other physiological systems subjected to
727 external demands for enhanced performance, can take a considerable period of
728 time to return to a stable baseline state.
729
730
731
732
733
734
735
736

```

<b>Notes:</b>	737
	738
	739
• maximum likelihood in the wavelet domain	740
	741
	742
<b>Wavelets and functional magnetic resonance imaging of the human brain - Bullmore et al. (2004) [56]</b>	743
	744
	745
	746
We provide a brief formal introduction to key properties of the DWT and review the growing literature on its application to fMRI. We focus on three applications in particular: (i) wavelet coefficient resampling or “wavestrapping” of 1-D time-series, 2- to 3-D spatial maps and 4-D spatiotemporal processes; (ii) wavelet-based estimators for signal and noise parameters of time-series regression models assuming the errors are fractional Gaussian noise (fGn); and (iii) wavelet shrinkage in frequentist and Bayesian frameworks to support multiresolution hypothesis testing on spatially extended statistic maps.	747
	748
	749
	750
	751
	752
	753
	754
	755
	756
	757
	758
<b>Notes:</b>	759
	760
	761
• This paper suggests that motion correction translates many fBm signals to fGn... however, it is not clear where this data comes from.	762
	763
	764
	765
	766
<b>Fractal-Based Analysis of fMRI BOLD Signal During Naturalistic Viewing Conditions - Campbell et al. (2021) [57]</b>	767
	768
	769
	770
We performed fractal analysis on Human Connectome Project 7T fMRI data ( $n = 72$ , 41 females, mean age $29.46 \pm 3.76$ years) to compare H across movie-watching and rest. Results: In contrast to previous work using conventional tasks, we found higher H values for movie relative to rest (mean difference = 0.014; $p = 5.279 \times 10^{-7}$ ; 95% CI [0.009, 0.019]). H was significantly higher in movie than rest in the visual, somatomotor and dorsal attention networks, but was significantly lower during movie in the frontoparietal and default networks. We found no cross-condition differences in test-retest reliability of	771
	772
	773
	774
	775
	776
	777
	778
	779
	780
	781
	782

783 H. Finally, we found that H of movie-derived stimulus properties (e.g., luminance changes)  
784 were fractal whereas H of head motion estimates were non-fractal.  
785

786

787 **Notes:**

788

789

790 •

791

792

793

794 **Scale-free brain dynamics under physical and psychological distress:**

795 **Pre-treatment effects in women diagnosed with breast cancer -**

796

797 **Churchill et al. (2015) [58]**

798

799 In a BOLD functional magnetic resonance imaging study, we scanned three groups during a  
800 working memory task: women scheduled to receive chemotherapy or radiotherapy and aged-  
801 matched controls. Surprisingly, patients' BOLD signal exhibited greater H with increasing  
802 intensity of anticipated treatment. However, an analysis of H and functional connectivity  
803 against self-reported measures of psychological distress (Worry, Anxiety, Depression) and  
804 physical distress (Fatigue, Sleep problems) revealed significant interactions. The modula-  
805 tion of (Worry, Anxiety) versus (Fatigue, Sleep Problems, Depression) showed the strongest  
806 effect, where higher worry and lower fatigue was related to reduced H in regions involved  
807 in visuospatial search, attention, and memory processing. This is also linked to decreased  
808 functional connectivity in these brain regions.

809

810

811 **Notes:**

812

813

814

815

816

817

818

819 **The suppression of scale-free fMRI brain dynamics across three**

820

821 **different sources of effort: Aging, task novelty and task difficulty -**

822

823 **Churchill et al. (2016) [37]**

824

825

826

827

828

Decreases in the Hurst exponent (H), which quantifies scale-free signal, was related to three  
different sources of cognitive effort/task engagement: 1) task difficulty, 2) task novelty,  
and 3) aging effects. These results were consistently observed across multiple datasets

and task paradigms. We also demonstrated that estimates of H are robust across a range of time-window sizes. H was also compared to alternative metrics of BOLD variability (SDBOLD) and global connectivity (Gconn), with effort-related decreases in H producing similar decreases in SDBOLD and Gconn.

**Notes:**

**Interplay between functional connectivity and scale-free dynamics in intrinsic fMRI networks - Ciuciu et al. (2014) [35]**

We applied this framework to fMRI data acquired from healthy young adults at rest and performing a visual detection task. First, we found that scale-invariance existed beyond univariate dynamics, being present also in bivariate cross-temporal dynamics. Second, we observed that frequencies within the scale-free range do not contribute evenly to interregional connectivity, with a systematically stronger contribution of the lowest frequencies, both at rest and during task. Third, in addition to a decrease of the Hurst exponent and inter-regional correlations, task performance modified cross-temporal dynamics, inducing a larger contribution of the highest frequencies within the scale-free range to global correlation. Lastly, we found that across individuals, a weaker task modulation of the frequency contribution to inter-regional connectivity was associated with better task performance manifesting as shorter and less variable reaction times. These findings bring together two related fields that have hitherto been studied separately – resting-state networks and scale-free dynamics, and show that scale-free dynamics of human brain activity manifest in cross-regional interactions as well.

**Notes:**

829  
830  
831  
832  
833  
834  
835  
836  
837  
838  
839  
840  
841  
842  
843  
844  
845  
846  
847  
848  
849  
850  
851  
852  
853  
854  
855  
856  
857  
858  
859  
860  
861  
862  
863  
864  
865  
866  
867  
868  
869  
870  
871  
872  
873  
874

875 **Temporal fractal analysis of the rs-BOLD signal identifies brain**  
876 **abnormalities in autism spectrum disorder - Dona et al. (2017) [43]**  
877

878     “It is important to mention here that fractal dimension estimation based on a disper-  
879     sional analysis is quite robust with respect to uncorrelated noise and does not require  
880     881     preprocessing”  
882

883

884

885 **Notes:**

886

887

- 888     • ASD = reduced FD = increased H;  
889     • rare study to properly define fGn vs fBm first?

890

891

892 **Fractal analysis of brain blood oxygenation level dependent (BOLD)**

893 **signals from children with mild traumatic brain injury (mTBI) -**

894     **Dona et al. (2017) [47]**  
895

896

897 **Notes:**

898

899

900

- 901     • children with mTBI; mTBI = reduced FD = increased H  
902     • rare study to properly define fGn vs fBm first?

903

904

905

906 **Hurst Exponent Analysis of Resting-State fMRI Signal Complexity**

907 **across the Adult Lifespan - Dong et al. (2018) [33]**

908

909

910     Region-wise and voxel-wise analyses were performed to investigate the effects of age, gen-  
911     der, and their interaction on complexity. In region-wise analysis, we found that the healthy  
912     913     aging is accompanied by a loss of complexity in frontal and parietal lobe and increased  
914     complexity in insula, limbic, and temporal lobe. Meanwhile, differences in HE between gen-  
915     916     ders were found to be significant in parietal lobe ( $p = 0.04$ , corrected). However, there was  
917     918     no interaction between gender and age. In voxel-wise analysis, the significant complexity  
919     decrease with aging was found in frontal and parietal lobe, and complexity increase was  
920

found in insula, limbic lobe, occipital lobe, and temporal lobe with aging. Meanwhile, differences in HE between genders were found to be significant in frontal, parietal, and limbic lobe. Furthermore, we found age and sex interaction in right parahippocampal gyrus ( $p = 0.04$ , corrected). Our findings reveal HE variations of the rs-fMRI signal across the human adult lifespan and show that HE may serve as a new parameter to assess healthy aging process.

**Notes:** 921  
922  
923  
924  
925  
926  
927  
928  
929  
930  
931  
932  
933

- They state that increase in age = decrease in complexity 934  
935  
936

**Pitfalls in fractal time-series analysis: fMRI BOLD as an exemplary case - Eke et al. (2012) [59]** 937  
938  
939  
940  
941  
942  
943

**Wavelet-Generalized Least Squares: A New BLU Estimator of Linear Regression Models with 1/f Errors - Fadili & Bullmore (2002) [60]** 944  
945  
946  
947  
948  
949  
950

**Not in one metric: Neuroticism modulates different resting state metrics within distinctive brain regions - Gentili et al. (2017) [61]** 951  
952  
953  
954  
955  
956  
957  
958  
959  
960  
961  
962  
963  
964  
965  
966

Metrics more related to the measurement of regional intrinsic brain activity (fALFF, ALFF and REHO), or that provide a parsimonious index of integrated and segregated brain activity (HE), were more broadly modulated in regions related to emotions and their regulation. Metrics related to connectivity were modulated across a wider network of areas. Overall, these results show that neuroticism affects distinct aspects of brain resting state activity.

967 **Notes:**

968

969

- 970 • “parsimonious index of integrated and segregated brain activity (HE)”

971

- 972 • HE was inversely correlated to neuroticism

973

974

975 **Proneness to social anxiety modulates neural complexity in the**

976

977 **absence of exposure: A resting state fMRI study using Hurst**

978

979 **exponent - Gentili et al. (2015) [62]**

980

981 Results from fALFF were highly consistent with those obtained using LSAS and BFNE  
982 to predict HE. Overall our data indicate that spontaneous brain activity is influenced by  
983 the degree of social anxiety, on a continuum and in the absence of social stimuli. These  
984 findings suggest that social anxiety is a trait characteristic that shapes brain activity and  
985 predisposes to different reactions in social contexts.

986

987

988 **Notes:**

989

990

991

992

- 993 • “A recent article (Rubin et al., 2013) analyzes the robustness of different algorithms  
994 with respect to possible fMRI artifacts and time-series lengths. In particular, the  
995 relevance of preprocessing steps as motion correction, detrending and filtering were  
996 evaluated both on simulated and real fMRI data, while other preprocessing steps  
997 like segmentation were not evaluated, although they may have an impact on”

998

- 999 • “The HE of fMRI time-series is generally higher in gray matter than in white matter  
1000 (Maxim et al., 2005), augments in the hippocampus with aging, and decreases with  
1001 cholinergic transmission enhancement (Wink et al., 2006)”

1002

- 1003 • “As pointed out by Maxim (Maxim et al., 2005), fMRI noise, after these pre-  
1004 processing steps, can be described as fGn.”

1005

1006

1007

1008

1009

1010

1011

1012

- “The HE of fMRI time-series is generally higher in gray matter than in white matter (Maxim et al., 2005), augments in the hippocampus with aging, and decreases with cholinergic transmission enhancement (Wink et al., 2006).” 1013  
1014  
1015  
1016  
1017
- “a reduction of HE has been observed in autistic and schizophrenic patients (Lai et al., 2010; Sokunbi et al., 2014)” 1018  
1019  
1020
- “Since the HE can describe long and short range memory dynamics, it has been proposed as a measure of online information-processing efficiency: higher HEs are related to long memory dynamics and to higher temporal redundancy and less freedom to vary (He, 2011).” 1021  
1022  
1023  
1024  
1025  
1026  
1027  
1028

### **Real-time fractal signal processing in the time domain. - Hartmann et al. (2013) [63]**

Here we introduce real-time variants of the Detrended Fluctuation Analysis (DFA) and the closely related Signal Summation Conversion (SSC) methods, which are suitable to estimate the fractal exponent in one pass.

### **Altered fractal dynamics of gait: Reduced stride-interval correlations with aging and Huntington’s disease. - Hausdoff et al. (1997) [64]**

#### **Notes:**

- Gait... not fMRI

### **Scale-Free Properties of the Functional Magnetic Resonance Imaging Signal during Rest and Task - He (2011) [36]**

its power-law exponent differentiates between brain networks and correlates with fMRI signal variance and brain glucose metabolism. Importantly, in parallel to brain electrical field potentials, the variance and power-law exponent of the fMRI signal decrease during

task activation, suggesting that the signal contains more long-range memory during rest and conversely is more efficient at online information processing during task. The scale-free properties of the fMRI signal and brain electrical field potentials bespeak their respective stationarity and nonstationarity. This suggests that neurovascular coupling mechanism is likely to contain a transformation from nonstationarity to stationarity.

The fMRI signal time course from each ROI was extracted for each subject and fMRI run. The normalized or non-normalized power spectrum of the fMRI signal was computed using the Bartlett smoothing procedure of deriving the power spectral function from the lagged autocorrelation or auto-covariance function, respectively (Jenkins and Watts, 1998). A Tukey window of 20 fMRI frame width was applied for additional smoothing. The power spectra were then averaged across runs and subjects and across homologous ROIs, resulting in an average power spectrum for each of 21 brain regions (Fig. 2A). Finally, to obtain the power-law exponent  $\beta$ , the  $<0.1$  Hz range of each average power spectrum was fit with a power-law function:  $P(f) \propto f^{-\beta}$  using a least-squares fit. Using the low-frequency range to fit the power-law exponent avoids aliasing artifact in higher-frequency range (we used TR of 2.16 s, hence Nyquist limit is 0.23 Hz) and yields reliable measurement of the scale-free distribution (Eke et al., 2002).

The DFA method has the particular advantage of being applicable to both stationary and nonstationary data. To analyze our fMRI data, window lengths of 5, 10, 19, 38, and 95 fMRI frames were chosen so that the number of frames in each run (190 after discarding the first four frames) is an integer multiple of the window length.

<b>Fractal characterization of complexity in dynamic signals:</b>	1105
<b>Application to cerebral hemodynamics - Herman (2009) [12]</b>	1106
<b>Identification of brain activity from fMRI data: Comparison of three fractal scaling analyses. - Hu (2006) [65]</b>	1107
<b>A shift to randomness of brain oscillations in people with autism.</b>	1108
<b>Lai (2010) [44]</b>	1109
Complex fractal scaling of fMRI time-series was found in both groups but globally there was a significant shift to randomness in the ASC (mean $H = .758$ , $SD = .045$ ) compared with neurotypical volunteers (mean $H = .788$ , $SD = .047$ ).	1110
<b>Extraversion is encoded by scale-free dynamics of default mode network. Lei (2013) [66]</b>	1111
<b>Fractional Gaussian noise, functional MRI and Alzheimer's disease.</b>	1112
<b>Maxim (2005) [41]</b>	1113
we adopted the Davies-Harte algorithm, which is both exact and fast, to generate the fGn simulations used here. For each value of $H = 0.1, \dots 0.9$ , we simulated 1000 realizations of fGn with 512 time-points in each series; we set $\omega^2 = 1$ for all simulations.	1114
<b>NOTES:</b>	1115
• This paper has the figure showing signal goes from fBm to fGn with proper motion regression	1116
<b>Decomposing multifractal crossovers. Nagy (2017) [67]</b>	1117
The NIRS and fMRI-BOLD low-frequency fluctuations were dominated by a multifractal component over an underlying biologically relevant random noise, thus forming a bimodal	1118

1151 signal. The crossover between the EEG signal components was found at the boundary  
1152 between the and bands, suggesting an independent generator for the multifractal  
1153 rhythm. The robust implementation of the SFD method should be regarded as essential  
1154 in the seamless processing of large volumes of bimodal fMRI-BOLD imaging data for the  
1155 topology of multifractal metrics free of the masking effect of the underlying random noise.  
1156  
1157  
1158  
1159

1160 **Optimizing complexity measures for FMRI data: Algorithm,  
1161 artifact, and sensitivity. Rubin (2013) [68]**  
1163

1164 Power-spectrum, Higuchi's fractal dimension, and generalized Hurst exponent based esti-  
1165 mates were most successful by all criteria; the poorest-performing measures were wavelet,  
1166 detrended fluctuation analysis, aggregated variance, and rescaled range. Our results clearly  
1167 demonstrate that decisions regarding choice of algorithm, signal processing, time-series  
1168 length, and scanner have a significant impact on the reliability and sensitivity of com-  
1169 plexity estimates. operating on the edge of chaos, complex systems position themselves  
1170 for optimal responsivity to inputs, as well as ability to maintain homeostatic regulation.  
1171 Daubechies wavelet based computations (Hdb) *have long computation times, are not sen-*  
1172 *sitive to spikes, and show poor sensitivity to activation, tissue type, and emotional content;*  
1173 *for these Daubechies wavelet based estimates the overall performance increases with the*  
1174 *wavelet order up to a point (Hdb8), and then deteriorates. HRS and HAV, performed poorly*  
1175 *across the board. In terms of image contrast, overlap with activation, and group differences,*  
1176 *HDFA performed poorly as well, with HDFA-S outperforming HDFA and HDFA-L, sug-*  
1177 *gesting that the bulk of useful information is found at shorter lags. The most consistently*  
1178 *successful measures were the powerspectrum based measures HFFT and HpWelch, with*  
1179 *the latter slightly outperforming the former while taking much longer to compute Second,*  
1180 *it appears that detrending, regressing out the global mean, and excluding low frequencies*  
1181 *improves agreement between complexity and activation. 300-600 time-points Finally, the*  
1182 *best measures to use are either the power-spectrum based ones (HFFT or HpWelch) on a*  
1183 *restricted frequency range (above ,0.01 Hz),*  
1184  
1185  
1186  
1187  
1188  
1189  
1190  
1191  
1192  
1193  
1194  
1195  
1196

<b>Mutual information identifies spurious Hurst phenomena in resting state EEG and fMRI data. von Wegner (2018) [69]</b>	1197
	1198
	1199
	1200
	1201
	1202
	1203
	1204
	1205
	1206
	1207
	1208
	1209
	1210
	1211
	1212
	1213
	1214
	1215
	1216
	1217
	1218
	1219
	1220
	1221
	1222
	1223
	1224
	1225
	1226
	1227
	1228
	1229
	1230
	1231
	1232
	1233
	1234
	1235
	1236
	1237
	1238
	1239
	1240
	1241
	1242

1243 **References**

1244

1245 [1] Koch HV. Sur Une Courbe Continue sans Tangente, Obtenue Par Une  
1246 Construction Géométrique Élémentaire. *Astron och Fys.* 1904;1:681–702.

1248

1249 [2] Koch H. Une Méthode Géométrique Élémentaire Pour l'étude de Certaines Ques-  
1250 tions de La Théorie Des Courbes Planes. *Acta Mathematica.* 1906;30(0):145–174.  
1252  
1253 <https://doi.org/10.1007/BF02418570>.

1254

1255 [3] Mandelbrot B. How Long Is the Coast of Britain? Statistical Self-Similarity and  
1256 Fractional Dimension. *Science.* 1967 May;156(3775):636–638. <https://doi.org/10.1126/science.156.3775.636>.

1260

1261 [4] Jayalalitha G, Shanthoshini Deviha V, Uthayakumar R. Fractal Model for  
1262 Blood Flow in Cardiovascular System. *Computers in Biology and Medicine.* 2008  
1263 Jun;38(6):684–693. <https://doi.org/10.1016/j.compbiomed.2008.03.002>.

1266

1267 [5] Ansell HS, Kovács IA. Unveiling Universal Aspects of the Cellular Anatomy of  
1268 the Brain. *Communications Physics.* 2024 Jun;7(1):184. <https://doi.org/10.1038/s42005-024-01665-y>.

1271

1272 [6] Riley MA, Bonnette S, Kuznetsov N, Wallot S, Gao J. A Tutorial Introduction  
1273 to Adaptive Fractal Analysis. *Frontiers in Physiology.* 2012;3. <https://doi.org/10.3389/fphys.2012.00371>.

1277

1278 [7] Csermely P. Weak Links: Stabilizers of Complex Systems from Proteins to Social  
1279 Networks. 1st ed. The Frontiers Collection. Berlin New York: Springer; 2006.

1281

1282 [8] Beggs JM. The Cortex and the Critical Point. 1st ed. Cambridge, MA: MIT  
1283 Press Direct; 2022.

1286

1287

1288

- [9] Bak P, Tang C, Wiesenfeld K. Self-Organized Criticality: An Explanation of the 1/  $f$  Noise. *Physical Review Letters*. 1987 Jul;59(4):381–384. <https://doi.org/10.1103/PhysRevLett.59.381>. 1289  
1290  
1291  
1292  
1293  
1294  
1295  
1296  
1297  
1298  
1299  
1300  
1301  
1302  
1303  
1304  
1305  
1306  
1307  
1308  
1309  
1310  
1311  
1312  
1313  
1314  
1315  
1316  
1317  
1318  
1319  
1320  
1321  
1322  
1323  
1324  
1325  
1326  
1327  
1328  
1329  
1330  
1331  
1332  
1333  
1334
- [10] Lipsitz LA. Loss of 'Complexity' and Aging: Potential Applications of Fractals and Chaos Theory to Senescence. *JAMA*. 1992 Apr;267(13):1806. <https://doi.org/10.1001/jama.1992.03480130122036>. 1289  
1290  
1291  
1292  
1293  
1294  
1295  
1296  
1297  
1298  
1299  
1300  
1301  
1302  
1303  
1304  
1305  
1306  
1307  
1308  
1309  
1310  
1311  
1312  
1313  
1314  
1315  
1316  
1317  
1318  
1319  
1320  
1321  
1322  
1323  
1324  
1325  
1326  
1327  
1328  
1329  
1330  
1331  
1332  
1333  
1334
- [11] Lipsitz LA. Dynamics of Stability: The Physiologic Basis of Functional Health and Frailty. *The Journals of Gerontology Series A: Biological Sciences and Medical Sciences*. 2002 Mar;57(3):B115–B125. <https://doi.org/10.1093/gerona/57.3.B115>. 1289  
1290  
1291  
1292  
1293  
1294  
1295  
1296  
1297  
1298  
1299  
1300  
1301  
1302  
1303  
1304  
1305  
1306  
1307  
1308  
1309  
1310  
1311  
1312  
1313  
1314  
1315  
1316  
1317  
1318  
1319  
1320  
1321  
1322  
1323  
1324  
1325  
1326  
1327  
1328  
1329  
1330  
1331  
1332  
1333  
1334
- [12] Herman P, Kocsis L, Eke A. Fractal Characterization of Complexity in Dynamic Signals: Application to Cerebral Hemodynamics. In: Walker JM, Hyder F, editors. *Dynamic Brain Imaging*. vol. 489. Totowa, NJ: Humana Press; 2009. p. 23–40. 1289  
1290  
1291  
1292  
1293  
1294  
1295  
1296  
1297  
1298  
1299  
1300  
1301  
1302  
1303  
1304  
1305  
1306  
1307  
1308  
1309  
1310  
1311  
1312  
1313  
1314  
1315  
1316  
1317  
1318  
1319  
1320  
1321  
1322  
1323  
1324  
1325  
1326  
1327  
1328  
1329  
1330  
1331  
1332  
1333  
1334
- [13] Mukli P, Nagy Z, Racz FS, Herman P, Eke A. Impact of Healthy Aging on Multifractal Hemodynamic Fluctuations in the Human Prefrontal Cortex. *Frontiers in Physiology*. 2018 Aug;9:1072. <https://doi.org/10.3389/fphys.2018.01072>. 1289  
1290  
1291  
1292  
1293  
1294  
1295  
1296  
1297  
1298  
1299  
1300  
1301  
1302  
1303  
1304  
1305  
1306  
1307  
1308  
1309  
1310  
1311  
1312  
1313  
1314  
1315  
1316  
1317  
1318  
1319  
1320  
1321  
1322  
1323  
1324  
1325  
1326  
1327  
1328  
1329  
1330  
1331  
1332  
1333  
1334
- [14] Werner G. Fractals in the Nervous System: Conceptual Implications for Theoretical Neuroscience. *Frontiers in Physiology*. 2010; <https://doi.org/10.3389/fphys.2010.00015>. 1289  
1290  
1291  
1292  
1293  
1294  
1295  
1296  
1297  
1298  
1299  
1300  
1301  
1302  
1303  
1304  
1305  
1306  
1307  
1308  
1309  
1310  
1311  
1312  
1313  
1314  
1315  
1316  
1317  
1318  
1319  
1320  
1321  
1322  
1323  
1324  
1325  
1326  
1327  
1328  
1329  
1330  
1331  
1332  
1333  
1334
- [15] Eke A, Herman P, Kocsis L, Kozak LR. Fractal Characterization of Complexity in Temporal Physiological Signals. *Physiological Measurement*. 2002 Feb;23(1):R1–R38. <https://doi.org/10.1088/0967-3334/23/1/201>. 1289  
1290  
1291  
1292  
1293  
1294  
1295  
1296  
1297  
1298  
1299  
1300  
1301  
1302  
1303  
1304  
1305  
1306  
1307  
1308  
1309  
1310  
1311  
1312  
1313  
1314  
1315  
1316  
1317  
1318  
1319  
1320  
1321  
1322  
1323  
1324  
1325  
1326  
1327  
1328  
1329  
1330  
1331  
1332  
1333  
1334

- 1335 [16] Hermán P, Kocsis L, Eke A. Fractal Branching Pattern in the Pial Vasculature  
1336 in the Cat. Journal of Cerebral Blood Flow and Metabolism: Official Jour-  
1337 nal of the International Society of Cerebral Blood Flow and Metabolism. 2001  
1338 Jun;21(6):741–753. <https://doi.org/10.1097/00004647-200106000-00012>.  
1341
- 1342 [17] Taylor R. Personal Reflections on Jackson Pollock's Fractal Paintings. História,  
1343 Ciências, Saúde-Manguinhos. 2006 Oct;13(suppl):109–123. <https://doi.org/10.1590/S0104-59702006000500007>.  
1347
- 1348 [18] Hurst HE. Long-Term Storage Capacity of Reservoirs. Transactions of the Amer-  
1349 ican Society of Civil Engineers. 1951 Jan;116(1):770–799. <https://doi.org/10.1061/TACEAT.0006518>.  
1351
- 1353 [19] Mandelbrot B. Une Classe de Processus Stochastiques Homothetiques Soi: Appli-  
1355 cation a Loi Climatologique de H. E. Hurst. Comptes Rendus Del academie Des  
1356 Sciences De Paris. 1965;240:3274–3277.  
1358
- 1359
- 1360 [20] Molz FJ, Liu HH, Szulga J. Fractional Brownian Motion and Fractional Gaussian  
1361 Noise in Subsurface Hydrology: A Review, Presentation of Fundamental Prop-  
1362 erties, and Extensions. Water Resources Research. 1997 Oct;33(10):2273–2286.  
1364
- 1365 <https://doi.org/10.1029/97WR01982>.  
1366
- 1367 [21] Korvin G. Fractal Models in the Earth Sciences. Amsterdam ; New York: Elsevier;  
1368 1992.  
1370
- 1371 [22] Park K, Willinger W, editors. Self-Similar Network Traffic and Performance  
1372 Evaluation. 1st ed. Wiley; 2000.  
1374
- 1375
- 1376 [23] Graves T, Gramacy R, Watkins N, Franzke C. A Brief History of Long Mem-  
1377 ory: Hurst, Mandelbrot and the Road to ARFIMA, 1951–1980. Entropy. 2017  
1378 Sep;19(9):437. <https://doi.org/10.3390/e19090437>.  
1380

- [24] Eke A, Hermán P, Bassingthwaigte J, Raymond G, Percival D, Cannon M, et al. Physiological Time Series: Distinguishing Fractal Noises from Motions. *Pflügers Archiv - European Journal of Physiology*. 2000 Feb;439(4):403–415. <https://doi.org/10.1007/s004249900135>. 1381  
1382  
1383  
1384  
1385  
1386  
1387  
1388  
1389  
1390  
1391  
1392  
1393  
1394  
1395  
1396  
1397  
1398  
1399  
1400  
1401  
1402  
1403  
1404  
1405  
1406  
1407  
1408  
1409  
1410  
1411  
1412  
1413  
1414  
1415  
1416  
1417  
1418  
1419  
1420  
1421  
1422  
1423  
1424  
1425  
1426
- [25] Shannon CE. Communication in the Presence of Noise. *Proceedings of the IRE*. 1949 Jan;37(1):10–21. <https://doi.org/10.1109/JRPROC.1949.232969>. 1388  
1389  
1390  
1391  
1392  
1393  
1394  
1395  
1396  
1397  
1398  
1399  
1400  
1401  
1402  
1403  
1404  
1405  
1406  
1407  
1408  
1409  
1410  
1411  
1412  
1413  
1414  
1415  
1416  
1417  
1418  
1419  
1420  
1421  
1422  
1423  
1424  
1425  
1426
- [26] Clauset A, Shalizi CR, Newman MEJ. Power-Law Distributions in Empirical Data. *SIAM Review*. 2009 Nov;51(4):661–703. <https://doi.org/10.1137/070710111>. 1388  
1389  
1390  
1391  
1392  
1393  
1394  
1395  
1396  
1397  
1398  
1399  
1400  
1401  
1402  
1403  
1404  
1405  
1406  
1407  
1408  
1409  
1410  
1411  
1412  
1413  
1414  
1415  
1416  
1417  
1418  
1419  
1420  
1421  
1422  
1423  
1424  
1425  
1426
- [27] Kolmogorov A. Sulla Determinazione Empirica Di Una Legge Di Distribuzione. *Giornale dell’Istituto Italiano degli Attuari*. 1933;4:83–91. 1388  
1389  
1390  
1391  
1392  
1393  
1394  
1395  
1396  
1397  
1398  
1399  
1400  
1401  
1402  
1403  
1404  
1405  
1406  
1407  
1408  
1409  
1410  
1411  
1412  
1413  
1414  
1415  
1416  
1417  
1418  
1419  
1420  
1421  
1422  
1423  
1424  
1425  
1426
- [28] Smirnov N. Table for Estimating the Goodness of Fit of Empirical Distributions. *The Annals of Mathematical Statistics*. 1948 Jun;19(2):279–281. <https://doi.org/10.1214/aoms/1177730256>. 1388  
1389  
1390  
1391  
1392  
1393  
1394  
1395  
1396  
1397  
1398  
1399  
1400  
1401  
1402  
1403  
1404  
1405  
1406  
1407  
1408  
1409  
1410  
1411  
1412  
1413  
1414  
1415  
1416  
1417  
1418  
1419  
1420  
1421  
1422  
1423  
1424  
1425  
1426
- [29] Peitgen HO. The Science of Fractal Images. New York, NY: Springer New York; 1988. 1388  
1389  
1390  
1391  
1392  
1393  
1394  
1395  
1396  
1397  
1398  
1399  
1400  
1401  
1402  
1403  
1404  
1405  
1406  
1407  
1408  
1409  
1410  
1411  
1412  
1413  
1414  
1415  
1416  
1417  
1418  
1419  
1420  
1421  
1422  
1423  
1424  
1425  
1426
- [30] Davies RB, Harte DS. Tests for Hurst Effect. *Biometrika*. 1987;74(1):95–101. <https://doi.org/10.1093/biomet/74.1.95>. 1388  
1389  
1390  
1391  
1392  
1393  
1394  
1395  
1396  
1397  
1398  
1399  
1400  
1401  
1402  
1403  
1404  
1405  
1406  
1407  
1408  
1409  
1410  
1411  
1412  
1413  
1414  
1415  
1416  
1417  
1418  
1419  
1420  
1421  
1422  
1423  
1424  
1425  
1426
- [31] Asmussen S. Stochastic Simulation with a View Towards Stochastic Processes. University of Aarhus, Centre for Mathematical Physics and Stochastics; 1998. 1388  
1389  
1390  
1391  
1392  
1393  
1394  
1395  
1396  
1397  
1398  
1399  
1400  
1401  
1402  
1403  
1404  
1405  
1406  
1407  
1408  
1409  
1410  
1411  
1412  
1413  
1414  
1415  
1416  
1417  
1418  
1419  
1420  
1421  
1422  
1423  
1424  
1425  
1426
- [32] Hosking JR. Modeling Persistence in Hydrological Time Series Using Fractional Differencing. *Water Resources Research*. 1984;20(12):1898–1908. 1388  
1389  
1390  
1391  
1392  
1393  
1394  
1395  
1396  
1397  
1398  
1399  
1400  
1401  
1402  
1403  
1404  
1405  
1406  
1407  
1408  
1409  
1410  
1411  
1412  
1413  
1414  
1415  
1416  
1417  
1418  
1419  
1420  
1421  
1422  
1423  
1424  
1425  
1426

- 1427 [33] Dong J, Jing B, Ma X, Liu H, Mo X, Li H. Hurst Exponent Analysis of  
1428 Resting-State fMRI Signal Complexity across the Adult Lifespan. *Frontiers in*  
1429 *Neuroscience*. 2018 Feb;12:34. <https://doi.org/10.3389/fnins.2018.00034>.
- 1430
- 1431
- 1432 [34] Wink AM, Bullmore E, Barnes A, Bernard F, Suckling J. Monofractal and Multi-  
1433 fractal Dynamics of Low Frequency Endogenous Brain Oscillations in Functional  
1434 MRI. *Human Brain Mapping*. 2008 Jul;29(7):791–801. <https://doi.org/10.1002/hbm.20593>.
- 1435
- 1436
- 1437
- 1438
- 1439
- 1440 [35] Ciuciu P, Abry P, He BJ. Interplay between Functional Connectivity and Scale-  
1441 Free Dynamics in Intrinsic fMRI Networks. *NeuroImage*. 2014 Jul;95:248–263.  
1442
- 1443
- 1444
- 1445
- 1446 [36] He BJ. Scale-Free Properties of the Functional Magnetic Resonance Imaging Sig-  
1447 nal during Rest and Task. *The Journal of Neuroscience*. 2011 Sep;31(39):13786–  
1448 13795. <https://doi.org/10.1523/JNEUROSCI.2111-11.2011>.
- 1449
- 1450
- 1451
- 1452 [37] Churchill NW, Spring R, Grady C, Cimprich B, Askren MK, Reuter-Lorenz PA,  
1453 et al. The Suppression of Scale-Free fMRI Brain Dynamics across Three Different  
1454 Sources of Effort: Aging, Task Novelty and Task Difficulty. *Scientific Reports*.  
1455
- 1456
- 1457 2016 Aug;6(1):30895. <https://doi.org/10.1038/srep30895>.
- 1458
- 1459
- 1460 [38] Wink AM, Bernard F, Salvador R, Bullmore E, Suckling J. Age and Cholinergic  
1461 Effects on Hemodynamics and Functional Coherence of Human Hippocampus.  
1462
- 1463
- 1464
- 1465
- 1466
- 1467 [39] Mella AE, Vanderwal T, Miller SP, Weber AM. Temporal Complexity of  
1468 the BOLD-signal in Preterm versus Term Infants. *Cerebral Cortex*. 2024  
1469 Oct;34(10):bhae426. <https://doi.org/10.1093/cercor/bhae426>.
- 1470
- 1471
- 1472

- [40] Campbell OL, Weber AM. Monofractal Analysis of Functional Magnetic Resonance Imaging: An Introductory Review. *Human Brain Mapping*. 2022 Jun;43(8):2693–2706. <https://doi.org/10.1002/hbm.25801>. 1473  
1474  
1475  
1476  
1477  
1478  
1479  
1480  
1481  
1482  
1483  
1484  
1485  
1486  
1487  
1488  
1489  
1490  
1491  
1492  
1493  
1494  
1495  
1496  
1497  
1498  
1499  
1500  
1501  
1502  
1503  
1504  
1505  
1506  
1507  
1508  
1509  
1510  
1511  
1512  
1513  
1514  
1515  
1516  
1517  
1518
- [41] Maxim V, Šendur L, Fadili J, Suckling J, Gould R, Howard R, et al. Fractional Gaussian Noise, Functional MRI and Alzheimer’s Disease. *NeuroImage*. 2005 Mar;25(1):141–158. <https://doi.org/10.1016/j.neuroimage.2004.10.044>. 1473  
1474  
1475  
1476  
1477  
1478  
1479  
1480  
1481  
1482  
1483  
1484  
1485  
1486  
1487  
1488  
1489  
1490  
1491  
1492  
1493  
1494  
1495  
1496  
1497  
1498  
1499  
1500  
1501  
1502  
1503  
1504  
1505  
1506  
1507  
1508  
1509  
1510  
1511  
1512  
1513  
1514  
1515  
1516  
1517  
1518
- [42] Warsi MA, Molloy W, Noseworthy MD. Correlating Brain Blood Oxygenation Level Dependent (BOLD) Fractal Dimension Mapping with Magnetic Resonance Spectroscopy (MRS) in Alzheimer’s Disease. *Magnetic Resonance Materials in Physics, Biology and Medicine*. 2012 Oct;25(5):335–344. <https://doi.org/10.1007/s10334-012-0312-0>. 1473  
1474  
1475  
1476  
1477  
1478  
1479  
1480  
1481  
1482  
1483  
1484  
1485  
1486  
1487  
1488  
1489  
1490  
1491  
1492  
1493  
1494  
1495  
1496  
1497  
1498  
1499  
1500  
1501  
1502  
1503  
1504  
1505  
1506  
1507  
1508  
1509  
1510  
1511  
1512  
1513  
1514  
1515  
1516  
1517  
1518
- [43] Dona O, Hall GB, Noseworthy MD. Temporal Fractal Analysis of the Rs-BOLD Signal Identifies Brain Abnormalities in Autism Spectrum Disorder. *PLOS ONE*. 2017 Dec;12(12):e0190081. <https://doi.org/10.1371/journal.pone.0190081>. 1473  
1474  
1475  
1476  
1477  
1478  
1479  
1480  
1481  
1482  
1483  
1484  
1485  
1486  
1487  
1488  
1489  
1490  
1491  
1492  
1493  
1494  
1495  
1496  
1497  
1498  
1499  
1500  
1501  
1502  
1503  
1504  
1505  
1506  
1507  
1508  
1509  
1510  
1511  
1512  
1513  
1514  
1515  
1516  
1517  
1518
- [44] Lai MC, Lombardo MV, Chakrabarti B, Sadek SA, Pasco G, Wheelwright SJ, et al. A Shift to Randomness of Brain Oscillations in People with Autism. *Biological Psychiatry*. 2010 Dec;68(12):1092–1099. <https://doi.org/10.1016/j.biopsych.2010.06.027>. 1473  
1474  
1475  
1476  
1477  
1478  
1479  
1480  
1481  
1482  
1483  
1484  
1485  
1486  
1487  
1488  
1489  
1490  
1491  
1492  
1493  
1494  
1495  
1496  
1497  
1498  
1499  
1500  
1501  
1502  
1503  
1504  
1505  
1506  
1507  
1508  
1509  
1510  
1511  
1512  
1513  
1514  
1515  
1516  
1517  
1518
- [45] Linke AC, Chen B, Olson L, Cordova M, Wilkinson M, Wang T, et al. Altered Development of the Hurst Exponent in the Medial Prefrontal Cortex in Preschoolers With Autism. *Biological Psychiatry: Cognitive Neuroscience and Neuroimaging*. 2024 Sep;p. S2451902224002714. <https://doi.org/10.1016/j.bpsc.2024.09.003>. 1473  
1474  
1475  
1476  
1477  
1478  
1479  
1480  
1481  
1482  
1483  
1484  
1485  
1486  
1487  
1488  
1489  
1490  
1491  
1492  
1493  
1494  
1495  
1496  
1497  
1498  
1499  
1500  
1501  
1502  
1503  
1504  
1505  
1506  
1507  
1508  
1509  
1510  
1511  
1512  
1513  
1514  
1515  
1516  
1517  
1518

- 1519 [46] Uscătescu LC, Hyatt CJ, Dunn J, Kronbichler M, Calhoun V, Corbera S, et al.:  
1520       Using the Excitation/Inhibition Ratio to Optimize the Classification of Autism  
1521       and Schizophrenia.  
1522  
1523  
1524  
1525 [47] Dona O, Noseworthy MD, DeMatteo C, Connolly JF. Fractal Analysis of Brain  
1526       Blood Oxygenation Level Dependent (BOLD) Signals from Children with Mild  
1527       Traumatic Brain Injury (mTBI). PLOS ONE. 2017 Jan;12(1):e0169647. <https://doi.org/10.1371/journal.pone.0169647>.  
1528  
1529  
1530  
1531  
1532 [48] Wei M, Qin J, Yan R, Li H, Yao Z, Lu Q. Identifying Major Depressive Disorder  
1533       Using Hurst Exponent of Resting-State Brain Networks. Psychiatry Research:  
1534       Neuroimaging. 2013 Dec;214(3):306–312. <https://doi.org/10.1016/j.psychresns.2013.09.008>.  
1535  
1536  
1537  
1538  
1539  
1540 [49] Jing B, Long Z, Liu H, Yan H, Dong J, Mo X, et al. Identifying Current  
1541       and Remitted Major Depressive Disorder with the Hurst Exponent: A Compar-  
1542       ative Study on Two Automated Anatomical Labeling Atlases. Oncotarget. 2017  
1543       Oct;8(52):90452–90464. <https://doi.org/10.18632/oncotarget.19860>.  
1544  
1545  
1546  
1547 [50] Sokunbi MO, Gradin VB, Waiter GD, Cameron GG, Ahearn TS, Murray AD,  
1548       et al. Nonlinear Complexity Analysis of Brain fMRI Signals in Schizophre-  
1549       nia. PLoS ONE. 2014 May;9(5):e95146. <https://doi.org/10.1371/journal.pone.0095146>.  
1550  
1551  
1552  
1553  
1554  
1555 [51] Lindquist MA, Geuter S, Wager TD, Caffo BS. Modular Preprocessing Pipelines  
1556       Can Reintroduce Artifacts into fMRI Data. Human Brain Mapping. 2019  
1557       Jun;40(8):2358–2376. <https://doi.org/10.1002/hbm.24528>.  
1558  
1559  
1560  
1561 [52] Tanabe J, Miller D, Tregellas J, Freedman R, Meyer FG. Comparison of  
1562       Detrending Methods for Optimal fMRI Preprocessing. NeuroImage. 2002  
1563  
1564

- Apr;15(4):902–907. <https://doi.org/10.1006/nimg.2002.1053>. 1565  
1566
- [53] Afshinpour B, Hosseini-Zadeh GA, Soltanian-Zadeh H. Nonparametric Trend 1567  
Estimation in the Presence of Fractal Noise: Application to fMRI Time-Series 1568  
Analysis. *Journal of Neuroscience Methods*. 2008 Jun;171(2):340–348. <https://doi.org/10.1016/j.jneumeth.2008.03.017>. 1569  
1570  
1571  
1572  
1573  
1574  
1575  
1576  
1577  
1578  
1579  
1580  
1581  
1582  
1583  
1584  
1585  
1586  
1587  
1588  
1589  
1590  
1591  
1592  
1593  
1594  
1595  
1596  
1597  
1598  
1599  
1600  
1601  
1602  
1603  
1604  
1605  
1606  
1607  
1608  
1609  
1610
- [54] Akhrif A, Romanos M, Domschke K, Schmitt-Boehrer A, Neufang S. Fractal 1575  
Analysis of BOLD Time Series in a Network Associated With Waiting Impulsivity. 1576  
*Frontiers in Physiology*. 2018 Oct;9:1378. <https://doi.org/10.3389/fphys.2018.01378>. 1577  
1578  
1579  
1580  
1581  
1582  
1583  
1584  
1585  
1586  
1587  
1588  
1589  
1590  
1591  
1592  
1593  
1594  
1595  
1596  
1597  
1598  
1599  
1600  
1601  
1602  
1603  
1604  
1605  
1606  
1607  
1608  
1609  
1610
- [55] Barnes A, Bullmore ET, Suckling J. Endogenous Human Brain Dynamics Recover 1582  
Slowly Following Cognitive Effort. *PLoS ONE*. 2009 Aug;4(8):e6626. <https://doi.org/10.1371/journal.pone.0006626>. 1583  
1584  
1585  
1586  
1587  
1588  
1589  
1590  
1591  
1592  
1593  
1594  
1595  
1596  
1597  
1598  
1599  
1600  
1601  
1602  
1603  
1604  
1605  
1606  
1607  
1608  
1609  
1610
- [56] Bullmore E, Fadili J, Maxim V, Şendur L, Whitcher B, Suckling J, et al. Wavelets 1588  
and Functional Magnetic Resonance Imaging of the Human Brain. *NeuroImage*. 1589  
2004 Jan;23:S234–S249. <https://doi.org/10.1016/j.neuroimage.2004.07.012>. 1590  
1591  
1592  
1593  
1594  
1595  
1596  
1597  
1598  
1599  
1600  
1601  
1602  
1603  
1604  
1605  
1606  
1607  
1608  
1609  
1610
- [57] Campbell O, Vanderwal T, Weber AM. Fractal-Based Analysis of fMRI BOLD 1594  
Signal During Naturalistic Viewing Conditions. *Frontiers in Physiology*. 2022 1595  
Jan;12:809943. <https://doi.org/10.3389/fphys.2021.809943>. 1596  
1597  
1598  
1599  
1600  
1601  
1602  
1603  
1604  
1605  
1606  
1607  
1608  
1609  
1610
- [58] Churchill NW, Cimprich B, Askren MK, Reuter-Lorenz PA, Jung MS, Peltier 1600  
S, et al. Scale-free Brain Dynamics under Physical and Psychological Distress: 1601  
Pre-treatment Effects in Women Diagnosed with Breast Cancer. *Human Brain 1602  
Mapping*. 2015 Mar;36(3):1077–1092. <https://doi.org/10.1002/hbm.22687>. 1603  
1604  
1605  
1606  
1607  
1608  
1609  
1610
- [59] Eke A. Pitfalls in Fractal Time Series Analysis: fMRI BOLD as an Exemplary 1607  
Case. *Frontiers in Physiology*. 2012;3. <https://doi.org/10.3389/fphys.2012.00417>. 1608  
1609  
1610

- 1611 [60] Fadili MJ, Bullmore ET. Wavelet-Generalized Least Squares: A New BLU  
1612 Estimator of Linear Regression Models with 1/f Errors. NeuroImage. 2002  
1613 Jan;15(1):217–232. <https://doi.org/10.1006/nimg.2001.0955>.
- 1614  
1615  
1616  
1617 [61] Gentili C, Cristea IA, Ricciardi E, Vanello N, Popita C, David D, et al. Not in One  
1618 Metric: Neuroticism Modulates Different Resting State Metrics within Distinctive  
1619 Brain Regions. Behavioural Brain Research. 2017 Jun;327:34–43. <https://doi.org/10.1016/j.bbr.2017.03.031>.
- 1620  
1621  
1622  
1623  
1624 [62] Gentili C, Vanello N, Cristea I, David D, Ricciardi E, Pietrini P. Proneness to  
1625 Social Anxiety Modulates Neural Complexity in the Absence of Exposure: A Rest-  
1626 ing State fMRI Study Using Hurst Exponent. Psychiatry Research: Neuroimaging.  
1627  
1628 2015 May;232(2):135–144. <https://doi.org/10.1016/j.psychresns.2015.03.005>.
- 1629  
1630  
1631  
1632 [63] Hartmann A, Mukli P, Nagy Z, Kocsis L, Hermán P, Eke A. Real-Time Fractal  
1633 Signal Processing in the Time Domain. Physica A: Statistical Mechanics and its  
1634 Applications. 2013 Jan;392(1):89–102. <https://doi.org/10.1016/j.physa.2012.08.002>.
- 1635  
1636  
1637  
1638  
1639 [64] Hausdorff JM, Mitchell SL, Firton R, Peng CK, Cudkowicz ME, Wei JY,  
1640 et al. Altered Fractal Dynamics of Gait: Reduced Stride-Interval Correlations  
1641 with Aging and Huntington’s Disease. Journal of Applied Physiology. 1997  
1642 Jan;82(1):262–269. <https://doi.org/10.1152/jappl.1997.82.1.262>.
- 1643  
1644  
1645  
1646  
1647 [65] Hu J, Lee J, Gao J, White KD, Crosson B. Identification of Brain Activity from  
1648 fMRI Data: Comparison of Three Fractal Scaling Analyses. In: 2006 IEEE/NLM  
1649 Life Science Systems and Applications Workshop. Bethesda, MD: IEEE; 2006. p.  
1650  
1651 1–2.
- 1652  
1653  
1654  
1655  
1656

- [66] Lei X, Zhao Z, Chen H. Extraversion Is Encoded by Scale-Free Dynamics of Default Mode Network. *NeuroImage*. 2013 Jul;74:52–57. <https://doi.org/10.1016/j.neuroimage.2013.02.020>. 1657  
1658  
1659  
1660  
1661  
1662  
1663  
1664  
1665  
1666  
1667  
1668  
1669  
1670  
1671  
1672  
1673  
1674  
1675  
1676  
1677  
1678  
1679  
1680  
1681  
1682  
1683  
1684  
1685  
1686  
1687  
1688  
1689  
1690  
1691  
1692  
1693  
1694  
1695  
1696  
1697  
1698  
1699  
1700  
1701  
1702
- [67] Nagy Z, Mukli P, Herman P, Eke A. Decomposing Multifractal Crossovers. *Frontiers in Physiology*. 2017 Jul;8:533. <https://doi.org/10.3389/fphys.2017.00533>. 1663  
1664  
1665  
1666  
1667  
1668  
1669  
1670  
1671  
1672  
1673  
1674  
1675  
1676  
1677  
1678  
1679  
1680  
1681  
1682  
1683  
1684  
1685  
1686  
1687  
1688  
1689  
1690  
1691  
1692  
1693  
1694  
1695  
1696  
1697  
1698  
1699  
1700  
1701  
1702
- [68] Rubin D, Fekete T, Mujica-Parodi LR. Optimizing Complexity Measures for fMRI Data: Algorithm, Artifact, and Sensitivity. *PLoS ONE*. 2013 May;8(5):e63448. <https://doi.org/10.1371/journal.pone.0063448>. 1669  
1670  
1671  
1672  
1673  
1674  
1675  
1676  
1677  
1678  
1679  
1680  
1681  
1682  
1683  
1684  
1685  
1686  
1687  
1688  
1689  
1690  
1691  
1692  
1693  
1694  
1695  
1696  
1697  
1698  
1699  
1700  
1701  
1702
- [69] Von Wegner F, Laufs H, Tagliazucchi E. Mutual Information Identifies Spurious Hurst Phenomena in Resting State EEG and fMRI Data. *Physical Review E*. 2018 Feb;97(2):022415. <https://doi.org/10.1103/PhysRevE.97.022415>. 1675  
1676  
1677  
1678  
1679  
1680  
1681  
1682  
1683  
1684  
1685  
1686  
1687  
1688  
1689  
1690  
1691  
1692  
1693  
1694  
1695  
1696  
1697  
1698  
1699  
1700  
1701  
1702

1703 **Appendix**

1704

1705

1706 **Python code**

1707

1708 **Sample python code for testing power-law scaling**

1709

```
1710 print("HELLO")
1711
```

1712

```
1713 , color="r", fontsize=14) ax[1][1].text(0.002, .002, r'$H=0.8
1714
```

1715

1716 **Gaussian noise vs Brownian motion**

1717

1718 Time-series that are scale-invariant come in two categories: fractional Gaussian noise  
1719

1720 (fGn) and fractional Brownian motion (fBm) Figure 7. fGn signals are stationary,  
1721

1722 meaning they tend to center themselves along a mean value over time. In contrast,  
1723

1724 fBm signals are non-stationary, and their values tend to wander away from the mean.  
1725

1726 fGn and fBm can easily be converted from one to the other: fGn to fBm by applying a  
1727

1728 successive summation between elements of the fGn series; and fBm to fGn by applying  
1729 successive differences between elements of a fBm series.  
1730

1731 This introduces the first method of measuring H of a time-series: using a log-log  
1732

1733 plot of its power spectral density (**?@fig-fourprop D and E**), calculating the linear-  
1734

1735 regression slope, and, depending on the slope angle, using one of two equations:  
1736

1737

$$H = \begin{cases} \frac{\beta+1}{2}, & \text{if } -1 < \beta < 1 \\ \frac{\beta-1}{2}, & \text{if } 1 < \beta < 3 \end{cases} \quad (8)$$

1742

1743

1744

1745

1746

1747

1748

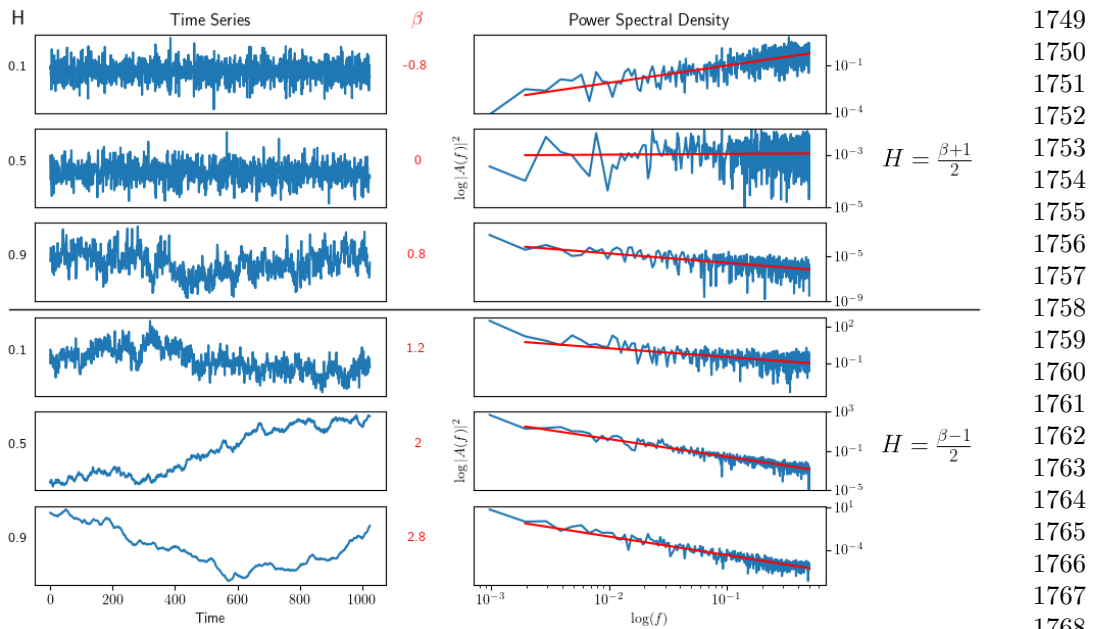


**Figure 5. Simulated fractional Gaussian noise and fractional Brownian motion.** Raw simulated time-series with 1,024 time-points and known Hurst values. Signals were created using the Davies-Harte method. a-c) are fractional Gaussian noise while d-f are fractional Brownian motion. a) and d) have  $H$  values of 0.1; b) and e) have  $H$  values of 0.5; and c) and f) have  $H$  values of 0.9. Note how fractional Gaussian noise remain centered around a mean (i.e. stationary), while fractional Brownian motion is free to wander (i.e. non-stationary). Exact fractal time-series were created using the Davies-Harte method.

If the class of signal is not appropriately identified — for example, when  $\beta$  is  $\sim 1$  — it is possible to seriously miscalculate the  $H$  value, such that a true  $H \sim 0.9$  will be calculated as 0.1. Therefore, algorithms and research in properly classifying fractal signals is crucially important.

1749  
1750  
1751  
1752  
1753  
1754  
1755  
1756  
1757  
1758  
1759  
1760  
1761  
1762  
1763  
1764  
1765  
1766  
1767  
1768  
1769  
1770  
1771  
1772  
1773  
1774  
1775  
1776  
1777  
1778  
1779  
1780  
1781  
1782  
1783  
1784  
1785  
1786  
1787  
1788  
1789  
1790  
1791  
1792  
1793  
1794

1795 **Prerequisites to measuring H**

1796

1797 **Time-points**

1798

1799 Before determining if a time-series exhibits a power-law scaling relationship, one  
1800 should first determine if the time-series has enough time-points to do so. The rule  
1802  
1803 of thumb is that the power law relationship should be present in a range larger  
1804 than two decades in the frequency domain of a PSD [24]. Due to the Whittaker–  
1805 Nyquist-Shannon sampling theorem [25], one requires two times as many time-points  
1807  
1808 as frequency samples. Since two decades in the frequency domain is 100 distinct  
1809 frequencies, one would required at least 200 time-points to proceed.  
1810

1811

1812 **Power-law scaling relationship**

1813

1814 The next step would be to perform a periodogram or PSD and test for a power-law  
1815  
1816 scaling relationship. Usually power laws are tested using a probability distribution  
1817  
1818 [26]. However, as the PSD is not a probability distribution, alternative methods must  
1819 be used. A goodness-of-fit test can be devised based on Clauset et al. [26], which can  
1820 also help us derive the SR (i.e.  $freq_{min}$  and  $freq_{max}$ ). First, a PSD is produced, and  
1822  
1823 the variance ( $\sigma^2$ ),  $\beta$ , and H are computed using Equation 8. Next, the Kolmogorov–  
1824 Smirnov statistic [27, 28] is used to measure the distance D between the raw PSD data-  
1825  
1826 points and the best-fit linear-regression line used to calculate H (i.e. the residuals).  
1827  
1828 The D in this case is the largest residual error. Then, 1,000 time series of either fGn  
1829  
1830 or fBm (depending on what value of  $\beta$  was found; see Equation 8) with the same  
1831 length ( $n > 200$ ),  $\sigma^2$ , and Hurst exponent are generated using one of several methods  
1832  
1833 for producing exact fractal signals: spectral synthesis method (SSM) [29], Davies–  
1834 Harte method (DH) [30], Cholesky method [31], or the Hosking’s method [32]. Each  
1835  
1836 synthetic time-series is converted to a PSD, and the Kolmogorov–Smirnov statistic  
1837  
1838 is used to measure the distance D between the raw PSD data-points and the best-fit  
1839 linear-regression line. The  $p$ -value is defined as the fraction of synthetic time series  
1840

with Ds that are larger than the original D of the original time-series. The larger the	1841
<i>p</i> -value, the more plausible the synthetic model (either fGn or fBm) is for representing	1842
the original time-series, and the better the fit of the original data to a scale-free	1843
distribution. The null-hypothesis that the time-series is not scale free is rejected if <i>p</i>	1844
< 0.05 (i.e. if <i>p</i> > 0.05, we say that the time-series is scale-free).	1845
	1846
	1847
	1848
	1849
However, this method can be computationally intensive, and prone to false negatives,	1850
especially signals with very high or low H values. One solution is, instead of applying	1851
this test to every voxel in a 4D fMRI brain scan, to segment the brain into separate	1852
ROIs (e.g. anatomically based on an atlas, or functionally by first running ICA to	1853
identify RSNs), average the time-series within each ROI, which will improve SNR,	1854
and then run the power-law scaling test.	1855
	1856
	1857
	1858
	1859
	1860
A sample python code is provide in Section 2	1861
	1862
<b>Scaling range</b>	1863
<b>fGn or fBm</b>	1864
<b>Choosing the right method</b>	1865
Ideally therefore, a long memory process signal should be categorized as either stationary	1866
(fGn) or non-stationary (fBm) and the variance and correlation defined. from [24]	1867
	1868
	1869
	1870
	1871
	1872
	1873
	1874
<b>Methods of measuring H</b>	1875
Fractal methods are diverse, but their approaches have one thing in common in that	1876
they employ equation (2) in fitting their proposed model to data pairs of log feature	1877
versus log scale for finding the scaling exponent, , from the regression slope. Each fractal	1878
analysis tool has different performance, prerequisite conditions, and limitations, and each	1879
needs thorough evaluation in order to avoid bias or misinterpretation of the derived fractal	1880
	1881
	1882
	1883
	1884
	1885
	1886

1887 parameters [5, 6, 8, 9], especially when applied to physiological signals which may be  
1888 contaminated with noise [15, 28]. from [24]  
1889

1890

1891 **Neuroscience Applications**

1892

1893 H has emerged as a valuable tool in neuroscience and clinical research. Typically, H  
1894 values reported in adult brains are above 0.5, with higher H values in grey matter  
1895 than white matter or cerebrospinal fluid [33, 34]. Some key findings from neuroscience  
1896 research include: a decrease in H during task performance [35, 36]; negative corre-  
1897 lations with task novelty and difficulty [37]; increases with age in the frontal and  
1898 parietal lobes [33], and hippocampus [38]; decreases with age in the insula, and lim-  
1899 bric, occipital and temporal lobes [33]; H < 0.5 in preterm infants [39]; and more [40].  
1900

1901 In terms of clinical findings, abnormal H values have been identified in Alzheimer's  
1902 disease (AD) [41, 42], autism spectrum disorder (ASD) [43–46], mild traumatic brain  
1903 injury [47], major depressive disorder [48, 49] and schizophrenia [46, 50].  
1904

1905

1906

1907 **fMRI preprocessing considerations**

1908

1909 **Nuissance regression**

1910

1911 When attempting to regress out non-BOLD signal, it is important to apply the regres-  
1912 sion at the same time, and not in succession. Even performing a band-pass filter after  
1913 nuissance regression can re-introduce noise components [51].  
1914

1915

1916 **Detrending**

1917

1918 see Tanabe et al. [52]

1919

1920

1921

1922

1923

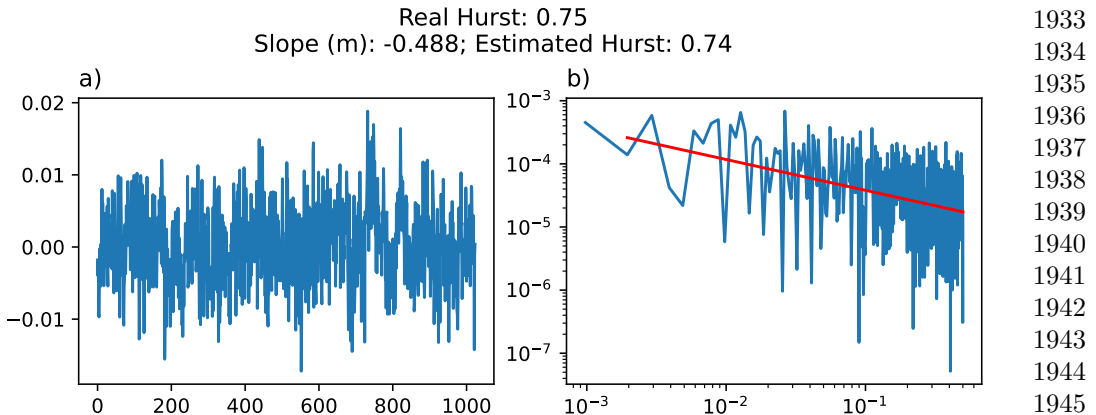


**Figure 6. Simulated fractional Gaussian noise.** a) Raw simulated time-series with 1,024 time-points and a known Hurst value of 0.75; b) The same signal from a) in a log-log power spectral density plot and a linear-regression used to calculate the estimated Hurst value.

## Hurst Reviews

**Nonparametric trend estimation in the presence of fractal noise:**

**Application to fMRI time-series analysis - Afshinpour et al. (2008)**

[53]

In this paper, a method for estimating trend in the presence of fractal noise is proposed and applied to fMRI time-series. To this end, a partly linear model (PLM) is fitted to each time-series. The parametric and nonparametric parts of PLM are considered as contributions of hemodynamic response and trend, respectively. Using the whitening property of wavelet transform, the unknown components of the model are estimated in the wavelet domain. The results of the proposed method are compared to those of other parametric trend-removal approaches such as spline and polynomial models. It is shown that the proposed method improves activation detection and decreases variance of the estimated parameters relative to the other methods.

**Notes:**

1979 • trend estimation paper  
 1980  
 1981 • 1.5T, 3.9x3.9x6mm, 1.648s TR, 256 time-points  
 1982 • Hurst method: Wavelet db4 with 5 scales  
 1983  
 1984  
 1985 **Fractal Analysis of BOLD time-series in a Network Associated With**  
 1986  
 1987 **Waiting Impulsivity - Akhrif et al. (2018) [54]**  
 1988  
 1989 examined **103** healthy male students at **rest** and while performing the 5-choice serial  
 1990 reaction time **task**. We addressed fractality in a network associated with waiting impulsiv-  
 1991 ity using the **adaptive fractal analysis (AFA)** approach to determine H. We revealed  
 1992 the fractal nature of the impulsivity network. Furthermore, fractality was influenced by  
 1993 individual impulsivity in terms of decreasing fractality (H) with higher impulsivity in  
 1994 regions of top-down control (left middle frontal gyrus) as well as reward processing (nucleus  
 1995 accumbens and anterior cingulate cortex).  
 1996  
 1997  
 1998  
 1999  
 2000  
 2001 **Notes:**  
 2002  
 2003  
 2004 • fMRI split into low and high frequency components. LFC is the second order  
 2005 polynomial that is a smooth and global fit of the original time course.  
 2006  
 2007 • AFA: variance of fluctuation computed around, in this case, a second order  
 2008 polynomial trend  $v(i)$  fitted to time-series within each segment  $w$ , and its size:  
 2009  
 2010  
 2011  
 2012  
 2013 
$$F(w) = \sqrt{\frac{1}{N} \sum_{i=1}^N (u(i) - v(i))^2} \sim w^H \quad (9)$$
  
 2014  
 2015  
 2016  $N$ : length of the time-series  
 2017  
 2018  
 2019  
 2020  $w = 2n + 1, n = 5, 6, \dots, 13$   
 2021  
 2022  
 2023 H is determined as the slope of the log-log plot  $\log_2(F(w))$  as a function of  $\log_2(w)$   
 2024

Example code:

```
import numpy as np  
  
def adaptive_fractal_analysis(signal, n_values=range(5, 14)):  
    """  
        Perform Adaptive Fractal Analysis (AFA) to compute the Hurst exponent.  
  
    Parameters:  
        signal (array-like): time-series data to analyze.  
        n_values (iterable): Sequence of `n` values to define window sizes as  $w = 2n + 1$ .  
  
    Returns:  
        float: Estimated Hurst exponent ( $H$ ).  
    """  
  
    # Define window sizes as  $w = 2n + 1$   
    window_sizes = [2 * n + 1 for n in n_values]  
    fluctuations = []  
  
    for window_size in window_sizes:  
        segment_variances = []  
        for start in range(0, len(signal) - window_size + 1, window_size):  
            # Extract the window  
            window = signal[start:start + window_size]  
            # Fit a second-order polynomial (quadratic fit) and compute residual  
            x = np.arange(len(window))  
            p = np.polyfit(x, window, deg=2)  # Degree 2 polynomial  
            residual = window - np.polyval(p, x)  
            segment_variances.append(np.var(residual))  
        fluctuations.append(np.sqrt(np.var(segment_variances)))  
  
    return fluctuations
```

```

2071     # Compute variance of the residuals
2072     variance = np.var(residual)
2073     segment_variances.append(variance)
2074
2075
2076
2077     # Compute average variance for this window size
2078     fluctuations.append(np.mean(segment_variances))
2079
2080
2081
2082     # Fit the scaling law: log(fluctuations) vs. log(window_sizes)
2083     log_window_sizes = np.log(window_sizes)
2084
2085     log_fluctuations = np.log(fluctuations)
2086
2087     slope, intercept = np.polyfit(log_window_sizes, log_fluctuations, deg=1)
2088
2089
2090
2091     # The slope corresponds to the Hurst exponent
2092
2093     return slope
2094
2095
2096 Endogenous human brain dynamics recover slowly following
2097
2098 cognitive effort - Barnes et al. (2009) [55]
2099
2100 1) Does performance of a cognitively effortful task significantly change fractal
2101 scaling properties of fMRI time-series compared to their values before task per-
2102 formance? 2) If so, can we relate the extent of task-related perturbation to the
2103 difficulty of the task? This result supports the model that endogenous low fre-
2104 quency oscillatory dynamics are relevant to the brain's response to exogenous
2105 stimulation. Moreover, it suggests that large-scale neurocognitive systems mea-
2106 sured using fMRI, like the heart and other physiological systems subjected to
2107 external demands for enhanced performance, can take a considerable period of
2108 time to return to a stable baseline state.
2109
2110
2111
2112
2113
2114
2115
2116

```

<b>Notes:</b>	2117
	2118
	2119
• maximum likelihood in the wavelet domain	2120
	2121
	2122
<b>Wavelets and functional magnetic resonance imaging of the human brain - Bullmore et al. (2004) [56]</b>	2123
	2124
	2125
	2126
We provide a brief formal introduction to key properties of the DWT and review the growing literature on its application to fMRI. We focus on three applications in particular: (i) wavelet coefficient resampling or “wavestrapping” of 1-D time-series, 2- to 3-D spatial maps and 4-D spatiotemporal processes; (ii) wavelet-based estimators for signal and noise parameters of time-series regression models assuming the errors are fractional Gaussian noise (fGn); and (iii) wavelet shrinkage in frequentist and Bayesian frameworks to support multiresolution hypothesis testing on spatially extended statistic maps.	2127
	2128
	2129
	2130
	2131
	2132
	2133
	2134
	2135
	2136
	2137
	2138
<b>Notes:</b>	2139
	2140
	2141
• This paper suggests that motion correction translates many fBm signals to fGn... however, it is not clear where this data comes from.	2142
	2143
	2144
	2145
	2146
<b>Fractal-Based Analysis of fMRI BOLD Signal During Naturalistic Viewing Conditions - Campbell et al. (2021) [57]</b>	2147
	2148
	2149
	2150
	2151
	2152
	2153
	2154
	2155
	2156
	2157
	2158
	2159
	2160
	2161
	2162

2163 H. Finally, we found that H of movie-derived stimulus properties (e.g., luminance changes)  
2164 were fractal whereas H of head motion estimates were non-fractal.  
2165

2166

2167 **Notes:**

2168

2169

2170 •

2171

2172

2173

2174 **Scale-free brain dynamics under physical and psychological distress:**

2175 **Pre-treatment effects in women diagnosed with breast cancer -**  
2176

2177 **Churchill et al. (2015) [58]**

2178

2179 In a BOLD functional magnetic resonance imaging study, we scanned three groups during a  
2180 working memory task: women scheduled to receive chemotherapy or radiotherapy and aged-  
2181 matched controls. Surprisingly, patients' BOLD signal exhibited greater H with increasing  
2182 intensity of anticipated treatment. However, an analysis of H and functional connectivity  
2183 against self-reported measures of psychological distress (Worry, Anxiety, Depression) and  
2184 physical distress (Fatigue, Sleep problems) revealed significant interactions. The modula-  
2185 tion of (Worry, Anxiety) versus (Fatigue, Sleep Problems, Depression) showed the strongest  
2186 effect, where higher worry and lower fatigue was related to reduced H in regions involved  
2187 in visuospatial search, attention, and memory processing. This is also linked to decreased  
2188 functional connectivity in these brain regions.

2189

2190

2191 **Notes:**

2192

2193

2194

2195

2196

2197

2198

2199 **The suppression of scale-free fMRI brain dynamics across three**

2200

2201 **different sources of effort: Aging, task novelty and task difficulty -**

2202

2203 **Churchill et al. (2016) [37]**

2204

2205

2206

2207

2208

Decreases in the Hurst exponent (H), which quantifies scale-free signal, was related to three  
different sources of cognitive effort/task engagement: 1) task difficulty, 2) task novelty,  
and 3) aging effects. These results were consistently observed across multiple datasets

and task paradigms. We also demonstrated that estimates of H are robust across a range  
of time-window sizes. H was also compared to alternative metrics of BOLD variability  
(SDBOLD) and global connectivity (Gconn), with effort-related decreases in H producing  
similar decreases in SDBOLD and Gconn.

**Notes:**

**Interplay between functional connectivity and scale-free dynamics in  
intrinsic fMRI networks - Ciuciu et al. (2014) [35]**

We applied this framework to fMRI data acquired from healthy young adults at rest and  
performing a visual detection task. First, we found that scale-invariance existed beyond  
univariate dynamics, being present also in bivariate cross-temporal dynamics. Second, we  
observed that frequencies within the scale-free range do not contribute evenly to interre-  
gional connectivity, with a systematically stronger contribution of the lowest frequencies,  
both at rest and during task. Third, in addition to a decrease of the Hurst exponent and  
inter-regional correlations, task performance modified cross-temporal dynamics, inducing  
a larger contribution of the highest frequencies within the scale-free range to global corre-  
lation. Lastly, we found that across individuals, a weaker task modulation of the frequency  
contribution to inter-regional connectivity was associated with better task performance  
manifesting as shorter and less variable reaction times. These findings bring together two  
related fields that have hitherto been studied separately – resting-state networks and scale-  
free dynamics, and show that scale-free dynamics of human brain activity manifest in  
cross-regional interactions as well.

**Notes:**

2255 **Temporal fractal analysis of the rs-BOLD signal identifies brain**  
2256  
2257 **abnormalities in autism spectrum disorder - Dona et al. (2017) [43]**  
2258  
2259 "It is important to mention here that fractal dimension estimation based on adisper-  
2260 sional analysis is quite robust with respect to uncorrelated noise and does not require  
2261 preprocessing"  
2263  
2264  
2265 **Notes:**  
2266  
2267  
2268 • ASD = reduced FD = increased H;  
2269 • rare study to properly define fGn vs fBm first?  
2271  
2272  
2273 **Fractal analysis of brain blood oxygenation level dependent (BOLD)**  
2274 **signals from children with mild traumatic brain injury (mTBI) -**  
2275  
2276 **Dona et al. (2017) [47]**  
2277  
2278 **Notes:**  
2279  
2280  
2281 • children with mTBI; mTBI = reduced FD = increased H  
2282  
2283 • rare study to properly define fGn vs fBm first?  
2284  
2285  
2286 **Hurst Exponent Analysis of Resting-State fMRI Signal Complexity**  
2287  
2288 **across the Adult Lifespan - Dong et al. (2018) [33]**  
2289  
2290 Region-wise and voxel-wise analyses were performed to investigate the effects of age, gen-  
2291 der, and their interaction on complexity. In region-wise analysis, we found that the healthy  
2292 aging is accompanied by a loss of complexity in frontal and parietal lobe and increased  
2293 complexity in insula, limbic, and temporal lobe. Meanwhile, differences in HE between gen-  
2294 ders were found to be significant in parietal lobe ( $p = 0.04$ , corrected). However, there was  
2297 no interaction between gender and age. In voxel-wise analysis, the significant complexity  
2298 decrease with aging was found in frontal and parietal lobe, and complexity increase was  
2300

found in insula, limbic lobe, occipital lobe, and temporal lobe with aging. Meanwhile, differences in HE between genders were found to be significant in frontal, parietal, and limbic lobe. Furthermore, we found age and sex interaction in right parahippocampal gyrus ( $p = 0.04$ , corrected). Our findings reveal HE variations of the rs-fMRI signal across the human adult lifespan and show that HE may serve as a new parameter to assess healthy aging process.

**Notes:**

- They state that increase in age = decrease in complexity

**Pitfalls in fractal time-series analysis: fMRI BOLD as an exemplary case - Eke et al. (2012) [59]**

**Wavelet-Generalized Least Squares: A New BLU Estimator of Linear Regression Models with 1/f Errors - Fadili & Bullmore (2002) [60]**

**Not in one metric: Neuroticism modulates different resting state metrics within distinctive brain regions - Gentili et al. (2017) [61]**

Metrics more related to the measurement of regional intrinsic brain activity (fALFF, ALFF and REHO), or that provide a parsimonious index of integrated and segregated brain activity (HE), were more broadly modulated in regions related to emotions and their regulation. Metrics related to connectivity were modulated across a wider network of areas. Overall, these results show that neuroticism affects distinct aspects of brain resting state activity.

2347 **Notes:**

2348

2349

2350 • “parsimonious index of integrated and segregated brain activity (HE)”

2351

2352 • HE was inversely correlated to neuroticism

2353

2354

2355 **Proneness to social anxiety modulates neural complexity in the**

2356

2357 **absence of exposure: A resting state fMRI study using Hurst**

2358

2359 **exponent - Gentili et al. (2015) [62]**

2360

2361 Results from fALFF were highly consistent with those obtained using LSAS and BFNE  
2362 to predict HE. Overall our data indicate that spontaneous brain activity is influenced by  
2363 the degree of social anxiety, on a continuum and in the absence of social stimuli. These  
2364 findings suggest that social anxiety is a trait characteristic that shapes brain activity and  
2365 predisposes to different reactions in social contexts.

2366

2367

2368 **Notes:**

2369

2370

2371

2372

2373 • “A recent article (Rubin et al., 2013) analyzes the robustness of different algorithms  
2374 with respect to possible fMRI artifacts and time-series lengths. In particular, the  
2375 relevance of preprocessing steps as motion correction, detrending and filtering were  
2376 evaluated both on simulated and real fMRI data, while other preprocessing steps  
2377 like segmentation were not evaluated, although they may have an impact on”

2378

2379 • “The HE of fMRI time-series is generally higher in gray matter than in white matter  
2380 (Maxim et al., 2005), augments in the hippocampus with aging, and decreases with  
2381 cholinergic transmission enhancement (Wink et al., 2006)”

2382

2383 • “As pointed out by Maxim (Maxim et al., 2005), fMRI noise, after these pre-  
2384 processing steps, can be described as fGn.”

2385

2386

2387

2388

2389

2390

2391

2392

• “The HE of fMRI time-series is generally higher in gray matter than in white matter (Maxim et al., 2005), augments in the hippocampus with aging, and decreases with cholinergic transmission enhancement (Wink et al., 2006).”	2393 2394 2395 2396 2397
• “a reduction of HE has been observed in autistic and schizophrenic patients (Lai et al., 2010; Sokunbi et al., 2014)”	2398 2399 2400
• “Since the HE can describe long and short range memory dynamics, it has been proposed as a measure of online information-processing efficiency: higher HEs are related to long memory dynamics and to higher temporal redundancy and less freedom to vary (He, 2011).”	2401 2402 2403 2404 2405 2406 2407 2408
<b>Real-time fractal signal processing in the time domain. - Hartmann et al. (2013) [63]</b>	2409 2410 2411 2412
Here we introduce real-time variants of the Detrended Fluctuation Analysis (DFA) and the closely related Signal Summation Conversion (SSC) methods, which are suitable to estimate the fractal exponent in one pass.	2413 2414 2415 2416 2417 2418 2419 2420
<b>Altered fractal dynamics of gait: Reduced stride-interval correlations with aging and Huntington’s disease. - Hausdoff et al. (1997) [64]</b>	2421 2422
<b>Notes:</b>	2423 2424 2425 2426 2427 2428 2429 2430
• Gait... not fMRI	2431 2432 2433 2434 2435 2436 2437 2438
<b>Scale-Free Properties of the Functional Magnetic Resonance Imaging Signal during Rest and Task - He (2011) [36]</b>	
its power-law exponent differentiates between brain networks and correlates with fMRI signal variance and brain glucose metabolism. Importantly, in parallel to brain electrical field potentials, the variance and power-law exponent of the fMRI signal decrease during	

2439 task activation, suggesting that the signal contains more long-range memory during rest  
2440 and conversely is more efficient at online information processing during task. The scale-free  
2441 properties of the fMRI signal and brain electrical field potentials bespeak their respective  
2442 stationarity and nonstationarity. This suggests that neurovascular coupling mechanism is  
2443 likely to contain a transformation from nonstationarity to stationarity.  
2444

2445  
2446  
2447  
2448 The fMRI signal time course from each ROI was extracted for each subject and fMRI  
2449 run. The normalized or non-normalized power spectrum of the fMRI signal was computed  
2450 using the Bartlett smoothing procedure of deriving the power spectral function from the  
2451 lagged autocorrelation or auto-covariance function, respectively (Jenkins and Watts, 1998).  
2452 A Tukey window of 20 fMRI frame width was applied for additional smoothing. The power  
2453 spectra were then averaged across runs and subjects and across homologous ROIs, resulting  
2454 in an average power spectrum for each of 21 brain regions (Fig. 2A). Finally, to obtain the  
2455 power-law exponent , the <0.1 Hz range of each average power spectrum was fit with a  
2456 power-law function:  $P(f) \propto 1/f^{\alpha}$  using a least-squares fit. Using the low-frequency range to  
2457 fit the power-law exponent avoids aliasing artifact in higher-frequency range (we used TR  
2458 of 2.16 s, hence Nyquist limit is 0.23 Hz) and yields reliable measurement of the scale-free  
2459 distribution (Eke et al., 2002).  
2460

2461  
2462  
2463  
2464  
2465  
2466  
2467 The DFA method has the particular advantage of being applicable to both stationary and  
2468 nonstationary data. To analyze our fMRI data, window lengths of 5, 10, 19, 38, and 95  
2469 fMRI frames were chosen so that the number of frames in each run (190 after discarding  
2470 the first four frames) is an integer multiple of the window length.  
2471

2472  
2473  
2474  
2475  
2476  
2477  
2478  
2479  
2480  
2481  
2482  
2483  
2484

<b>Fractal characterization of complexity in dynamic signals:</b>	2485
<b>Application to cerebral hemodynamics - Herman (2009) [12]</b>	2486
	2487
	2488
<b>Identification of brain activity from fMRI data: Comparison of three fractal scaling analyses. - Hu (2006) [65]</b>	2489
	2490
	2491
	2492
<b>A shift to randomness of brain oscillations in people with autism.</b>	2493
<b>Lai (2010) [44]</b>	2494
	2495
	2496
Complex fractal scaling of fMRI time-series was found in both groups but globally there was a significant shift to randomness in the ASC (mean $H = .758$ , $SD = .045$ ) compared with neurotypical volunteers (mean $H = .788$ , $SD = .047$ ).	2497
	2498
	2499
	2500
	2501
	2502
<b>Extraversion is encoded by scale-free dynamics of default mode network. Lei (2013) [66]</b>	2503
	2504
	2505
	2506
<b>Fractional Gaussian noise, functional MRI and Alzheimer's disease.</b>	2507
<b>Maxim (2005) [41]</b>	2508
	2509
	2510
we adopted the Davies-Harte algorithm, which is both exact and fast, to generate the fGn simulations used here. For each value of $H = 0.1, \dots, 0.9$ , we simulated 1000 realizations of fGn with 512 time-points in each series; we set $\omega^2 = 1$ for all simulations.	2511
	2512
	2513
	2514
	2515
	2516
<b>NOTES:</b>	2517
	2518
	2519
• This paper has the figure showing signal goes from fBm to fGn with proper motion regression	2520
	2521
	2522
	2523
	2524
<b>Decomposing multifractal crossovers. Nagy (2017) [67]</b>	2525
	2526
The NIRS and fMRI-BOLD low-frequency fluctuations were dominated by a multifractal component over an underlying biologically relevant random noise, thus forming a bimodal	2527
	2528
	2529
	2530

2531 signal. The crossover between the EEG signal components was found at the boundary  
2532 between the and bands, suggesting an independent generator for the multifractal  
2533 rhythm. The robust implementation of the SFD method should be regarded as essential  
2534 in the seamless processing of large volumes of bimodal fMRI-BOLD imaging data for the  
2535 topology of multifractal metrics free of the masking effect of the underlying random noise.  
2536  
2537  
2538  
2539

2540 **Optimizing complexity measures for fMRI data: Algorithm,  
2541 artifact, and sensitivity. Rubin (2013) [68]**  
2543

2544 Power-spectrum, Higuchi's fractal dimension, and generalized Hurst exponent based esti-  
2545 mates were most successful by all criteria; the poorest-performing measures were wavelet,  
2546 detrended fluctuation analysis, aggregated variance, and rescaled range. Our results clearly  
2547 demonstrate that decisions regarding choice of algorithm, signal processing, time-series  
2548 length, and scanner have a significant impact on the reliability and sensitivity of com-  
2549 plexity estimates. operating on the edge of chaos, complex systems position themselves  
2550 for optimal responsivity to inputs, as well as ability to maintain homeostatic regulation.  
2551 Daubechies wavelet based computations (Hdb) *have long computation times, are not sen-*  
2552 *sitive to spikes, and show poor sensitivity to activation, tissue type, and emotional content;*  
2553 *for these Daubechies wavelet based estimates the overall performance increases with the*  
2554 *wavelet order up to a point (Hdb8), and then deteriorates. HRS and HAV, performed poorly*  
2555 *across the board. In terms of image contrast, overlap with activation, and group differences,*  
2556 *HDFA performed poorly as well, with HDFA-S outperforming HDFA and HDFA-L, sug-*  
2557 *gesting that the bulk of useful information is found at shorter lags. The most consistently*  
2558 *successful measures were the powerspectrum based measures HFFT and HpWelch, with*  
2559 *the latter slightly outperforming the former while taking much longer to compute Second,*  
2560 *it appears that detrending, regressing out the global mean, and excluding low frequencies*  
2561 *improves agreement between complexity and activation. 300-600 time-points Finally, the*  
2562 *best measures to use are either the power-spectrum based ones (HFFT or HpWelch) on a*  
2563 *restricted frequency range (above ,0.01 Hz),*  
2564  
2565  
2566  
2567  
2568  
2569  
2570  
2571  
2572  
2573  
2574  
2575  
2576

<b>Mutual information identifies spurious Hurst phenomena in resting state EEG and fMRI data. von Wegner (2018) [69]</b>	2577
	2578
	2579
	2580
	2581
	2582
	2583
	2584
	2585
	2586
	2587
	2588
	2589
	2590
	2591
	2592
	2593
	2594
	2595
	2596
	2597
	2598
	2599
	2600
	2601
	2602
	2603
	2604
	2605
	2606
	2607
	2608
	2609
	2610
	2611
	2612
	2613
	2614
	2615
	2616
	2617
	2618
	2619
	2620
	2621
	2622

## 2623 **References**

2624

2625

2626

2627

2628

2629

2630

2631

2632

2633

2634

2635

2636

2637

2638

2639

2640

2641

2642

2643

2644

2645

2646

2647

2648

2649

2650

2651

2652

2653

2654

2655

2656

2657

2658

2659

2660

2661

2662

2663

2664

2665

2666

2667

2668

<b>Appendix</b>	2669
	2670
<b>Python code</b>	2671
	2672
	2673
	2674
<b>Sample python code for testing power-law scaling</b>	2675
	2676
<b>print("HELLO")</b>	2677
	2678
,   color="r",   fontsize=14)   ax[1][1].set_title("Log-log plot of D",   loc='left')	2679
ax[1][1].set_xlabel('Frequency (f)') ax[1][1].set_ylabel(r'Amplitude ( $ A(f) ^2$ )')	2680
	2681
newpower=power fp5 = FBM(scale1, hurst=0.5, length=1, method='daviesharte')	2682
fgnp5   =   fp5.fgn()5   p5freq,   p5power   =   signal.periodogram(fgnp5,   1)	2683
p5power=p5power - np.mean(p5power) + predicted_power[-1]/1.4 newpower[:10]=	2684
(np.random.rand(10)+0.5) # 10 was the power value around the low frequency	2685
newpower[312:] = p5power[312:512]    ax[2][1].plot(freq.reshape(-1,1),    newpower)	2686
ax[2][1].plot(freq[1:].reshape(-1,1)[10:312],   predicted_power[10:312],   color='red')	2687
ax[2][1].axvline(x=freq[10],   color='red',   linestyle='--')   ax[2][1].axvline(x=freq[312],	2688
color='red',   linestyle='--')   ax[2][1].set_xscale('log')   ax[2][1].set_yscale('log')	2689
ax[2][1].set_xlabel('Frequency (f)') ax[2][1].set_title("E but with a scaling range",	2690
loc='left')	2691
	2692
text_xy = (freq[10]*1.7,  0.001) ax[2][1].annotate(text, (freq[10],0.001), text_xy,	2693
arrowprops={"arrowstyle": "->", "color": "red"}, color="red") ax[2][1].annotate(text,	2694
(freq[312],0.001),  text_xy,  arrowprops={"arrowstyle": "->",  "color": "red"},	2695
color="red")	2696
	2697
for i   in  range(3):  ax[i,  0].text(-0.1,  1.1,  string.ascii_uppercase[i],  trans-	2698
form=ax[i,  0].transAxes,  size=13,  weight='bold')  ax[i,  1].text(-0.1,  1.1,	2699
string.ascii_uppercase[i+3], transform=ax[i, 1].transAxes, size=13, weight='bold')	2700
	2701
	2702
	2703
	2704
	2705
	2706
	2707
	2708
	2709
	2710
	2711
	2712
	2713
	2714

```

2715 plt.savefig('..../image/fourproperties.png', dpi=600, bbox_inches='tight',
2716 format='png') plt.show()
2718
2719
2720
2721 :::.cell-output .cell-output-display}
2722 ! [I don't get why this isn't working] (index_files/figure-latex/notebooks-Figures-fig-fourp
2723
2724 :::
2725
2726 :::
2727
2728
2729
2730
2731
2732
2733
2734 :::
2735
2736
2737
2738
2739
2740
2741
2742
2743
2744
2745
2746
2747 ## Gaussian noise vs Brownian motion
2748
2749
2750
2751 Time-series that are scale-invariant come in two categories: fractional Gaussian noise (fG
2752
2753
2754 <!-- TODO: find where to put this: -->
2755
2756 This introduces the first method of measuring H of a time-series: using a log-log plot of
2757
2758
2759 $$
2760

```

```

H =
2761
\begin{cases}
2762
\frac{\beta + 1}{2}, & \text{if } -1 < \beta < 1 \\
2764
\frac{\beta - 1}{2}, & \text{if } 1 < \beta < 3
2765
\end{cases}
2766
\$ \$ \{\#eq-psdH\}
2767
2768
2769
2770
2771
2772
2773
2774
2775
2776
2777
2778
2779
2780
2781
2782
2783
2784
2785
2786
2787
2788
2789
2790
2791
2792
2793
2794
2795
2796
2797
2798
2799
2800
2801
2802
2803
2804
2805
2806
:::{.quarto-embed-nb-cell notebook="/home/weberam2/Dropbox/AssistantProf_B2MRI/Projects/Brainl
::: {.cell execution_count=19}
``` {.python .cell-code .hidden}
np.random.seed(1)
plt.rcParams['text.usetex'] = True #latex
def psd(timeseries):
    freq, power = signal.periodogram(timeseries, 1)
    power = power[1:]
    freq = freq[1:]

    log_power = np.log10(power)
    log_freq = np.log10(freq)
    log_power = log_power[1:]

```

```

2807     log_freq = log_freq[1:]
2808
2809
2810     model = LinearRegression()
2811
2812     model.fit(log_freq.reshape(-1,1), log_power)
2813
2814     predicted_power = 10**model.predict(log_freq.reshape(-1,1))
2815
2816
2817     return freq.reshape(-1,1), power, predicted_power
2818
2819
2820 fp5 = FBM(1024, hurst=0.5, length=1, method='daviesharte')
2821
2822 fp1 = FBM(1024, hurst=0.1, length=1, method='daviesharte')
2823
2824 fp9 = FBM(1024, hurst=0.9, length=1, method='daviesharte')
2825
2826 fgnp5 = fp5.fgn()
2827
2828 fgnp1 = fp1.fgn()
2829
2830 fgnp9 = fp9.fgn()
2831
2832 fbmp5 = fp5.fbm()
2833
2834 fbmp1 = fp1.fbm()
2835
2836 fbmp9 = fp9.fbm()
2837
2838
2839 fig, ax = plt.subplots(6,2, figsize=(10,7))
2840
2841 fig.subplots_adjust(wspace=0.25)
2842
2843 ax[0,0].plot(fgnp1)
2844
2845 ax[0,0].set_title("Time Series")
2846
2847 ax[0,0].xaxis.set_visible(False)
2848
2849 ax[0,0].set_ylabel("0.1", rotation=0, labelpad=12)
2850
2851 ax[0,0].text(1.05, 0.55, "-0.8", rotation=0,
2852
2853
2854
2855
2856
2857
2858
2859
2860
2861
2862
2863
2864
2865
2866
2867
2868
2869
2870
2871
2872
2873
2874
2875
2876
2877
2878
2879
2880
2881
2882
2883
2884
2885
2886
2887
2888
2889
2890
2891
2892
2893
2894
2895
2896
2897
2898
2899
2900
2901
2902
2903
2904
2905
2906
2907
2908
2909
2910
2911
2912
2913
2914
2915
2916
2917
2918
2919
2920
2921
2922
2923
2924
2925
2926
2927
2928
2929
2930
2931
2932
2933
2934
2935
2936
2937
2938
2939
2940
2941
2942
2943
2944
2945
2946
2947
2948
2949
2950
2951
2952
2953
2954
2955
2956
2957
2958
2959
2960
2961
2962
2963
2964
2965
2966
2967
2968
2969
2970
2971
2972
2973
2974
2975
2976
2977
2978
2979
2980
2981
2982
2983
2984
2985
2986
2987
2988
2989
2990
2991
2992
2993
2994
2995
2996
2997
2998
2999
3000
3001
3002
3003
3004
3005
3006
3007
3008
3009
3010
3011
3012
3013
3014
3015
3016
3017
3018
3019
3020
3021
3022
3023
3024
3025
3026
3027
3028
3029
3030
3031
3032
3033
3034
3035
3036
3037
3038
3039
3040
3041
3042
3043
3044
3045
3046
3047
3048
3049
3050
3051
3052
3053
3054
3055
3056
3057
3058
3059
3060
3061
3062
3063
3064
3065
3066
3067
3068
3069
3070
3071
3072
3073
3074
3075
3076
3077
3078
3079
3080
3081
3082
3083
3084
3085
3086
3087
3088
3089
3090
3091
3092
3093
3094
3095
3096
3097
3098
3099
3100
3101
3102
3103
3104
3105
3106
3107
3108
3109
3110
3111
3112
3113
3114
3115
3116
3117
3118
3119
3120
3121
3122
3123
3124
3125
3126
3127
3128
3129
3130
3131
3132
3133
3134
3135
3136
3137
3138
3139
3140
3141
3142
3143
3144
3145
3146
3147
3148
3149
3150
3151
3152
3153
3154
3155
3156
3157
3158
3159
3160
3161
3162
3163
3164
3165
3166
3167
3168
3169
3170
3171
3172
3173
3174
3175
3176
3177
3178
3179
3180
3181
3182
3183
3184
3185
3186
3187
3188
3189
3190
3191
3192
3193
3194
3195
3196
3197
3198
3199
3200
3201
3202
3203
3204
3205
3206
3207
3208
3209
3210
3211
3212
3213
3214
3215
3216
3217
3218
3219
3220
3221
3222
3223
3224
3225
3226
3227
3228
3229
3230
3231
3232
3233
3234
3235
3236
3237
3238
3239
3240
3241
3242
3243
3244
3245
3246
3247
3248
3249
3250
3251
3252
3253
3254
3255
3256
3257
3258
3259
3260
3261
3262
3263
3264
3265
3266
3267
3268
3269
3270
3271
3272
3273
3274
3275
3276
3277
3278
3279
3280
3281
3282
3283
3284
3285
3286
3287
3288
3289
3290
3291
3292
3293
3294
3295
3296
3297
3298
3299
3300
3301
3302
3303
3304
3305
3306
3307
3308
3309
3310
3311
3312
3313
3314
3315
3316
3317
3318
3319
3320
3321
3322
3323
3324
3325
3326
3327
3328
3329
3330
3331
3332
3333
3334
3335
3336
3337
3338
3339
3340
3341
3342
3343
3344
3345
3346
3347
3348
3349
3350
3351
3352
3353
3354
3355
3356
3357
3358
3359
3360
3361
3362
3363
3364
3365
3366
3367
3368
3369
3370
3371
3372
3373
3374
3375
3376
3377
3378
3379
3380
3381
3382
3383
3384
3385
3386
3387
3388
3389
3390
3391
3392
3393
3394
3395
3396
3397
3398
3399
3400
3401
3402
3403
3404
3405
3406
3407
3408
3409
3410
3411
3412
3413
3414
3415
3416
3417
3418
3419
3420
3421
3422
3423
3424
3425
3426
3427
3428
3429
3430
3431
3432
3433
3434
3435
3436
3437
3438
3439
3440
3441
3442
3443
3444
3445
3446
3447
3448
3449
3450
3451
3452
3453
3454
3455
3456
3457
3458
3459
3460
3461
3462
3463
3464
3465
3466
3467
3468
3469
3470
3471
3472
3473
3474
3475
3476
3477
3478
3479
3480
3481
3482
3483
3484
3485
3486
3487
3488
3489
3490
3491
3492
3493
3494
3495
3496
3497
3498
3499
3500
3501
3502
3503
3504
3505
3506
3507
3508
3509
3510
3511
3512
3513
3514
3515
3516
3517
3518
3519
3520
3521
3522
3523
3524
3525
3526
3527
3528
3529
3530
3531
3532
3533
3534
3535
3536
3537
3538
3539
3540
3541
3542
3543
3544
3545
3546
3547
3548
3549
3550
3551
3552
3553
3554
3555
3556
3557
3558
3559
3560
3561
3562
3563
3564
3565
3566
3567
3568
3569
3570
3571
3572
3573
3574
3575
3576
3577
3578
3579
3580
3581
3582
3583
3584
3585
3586
3587
3588
3589
3590
3591
3592
3593
3594
3595
3596
3597
3598
3599
3600
3601
3602
3603
3604
3605
3606
3607
3608
3609
3610
3611
3612
3613
3614
3615
3616
3617
3618
3619
3620
3621
3622
3623
3624
3625
3626
3627
3628
3629
3630
3631
3632
3633
3634
3635
3636
3637
3638
3639
3640
3641
3642
3643
3644
3645
3646
3647
3648
3649
3650
3651
3652
3653
3654
3655
3656
3657
3658
3659
3660
3661
3662
3663
3664
3665
3666
3667
3668
3669
3670
3671
3672
3673
3674
3675
3676
3677
3678
3679
3680
3681
3682
3683
3684
3685
3686
3687
3688
3689
3690
3691
3692
3693
3694
3695
3696
3697
3698
3699
3700
3701
3702
3703
3704
3705
3706
3707
3708
3709
3710
3711
3712
3713
3714
3715
3716
3717
3718
3719
3720
3721
3722
3723
3724
3725
3726
3727
3728
3729
3730
3731
3732
3733
3734
3735
3736
3737
3738
3739
3740
3741
3742
3743
3744
3745
3746
3747
3748
3749
3750
3751
3752
3753
3754
3755
3756
3757
3758
3759
3760
3761
3762
3763
3764
3765
3766
3767
3768
3769
3770
3771
3772
3773
3774
3775
3776
3777
3778
3779
3780
3781
3782
3783
3784
3785
3786
3787
3788
3789
3790
3791
3792
3793
3794
3795
3796
3797
3798
3799
3800
3801
3802
3803
3804
3805
3806
3807
3808
3809
3810
3811
3812
3813
3814
3815
3816
3817
3818
3819
3820
3821
3822
3823
3824
3825
3826
3827
3828
3829
3830
3831
3832
3833
3834
3835
3836
3837
3838
3839
3840
3841
3842
3843
3844
3845
3846
3847
3848
3849
3850
3851
3852
3853
3854
3855
3856
3857
3858
3859
3860
3861
3862
3863
3864
3865
3866
3867
3868
3869
3870
3871
3872
3873
3874
3875
3876
3877
3878
3879
3880
3881
3882
3883
3884
3885
3886
3887
3888
3889
3890
3891
3892
3893
3894
3895
3896
3897
3898
3899
3900
3901
3902
3903
3904
3905
3906
3907
3908
3909
3910
3911
3912
3913
3914
3915
3916
3917
3918
3919
3920
3921
3922
3923
3924
3925
3926
3927
3928
3929
3930
3931
3932
3933
3934
3935
3936
3937
3938
3939
3940
3941
3942
3943
3944
3945
3946
3947
3948
3949
3950
3951
3952
3953
3954
3955
3956
3957
3958
3959
3960
3961
3962
3963
3964
3965
3966
3967
3968
3969
3970
3971
3972
3973
3974
3975
3976
3977
3978
3979
3980
3981
3982
3983
3984
3985
3986
3987
3988
3989
3990
3991
3992
3993
3994
3995
3996
3997
3998
3999
3999

```

```

ax[1,0].plot(fgnp5)                                     2853
ax[1,0].xaxis.set_visible(False)                         2854
ax[1,0].set_yticks([])                                  2855
ax[1,0].set_ylabel("0.5", rotation=0, labelpad=12)       2856
ax[1,0].text(1.08, 0.55, "0", rotation=0,               2857
             transform=ax[1,0].transAxes, color='red')      2858
ax[2,0].plot(fgnp9)                                     2859
ax[2,0].xaxis.set_visible(False)                         2860
ax[2,0].set_yticks([])                                  2861
ax[2,0].set_ylabel("0.9", rotation=0, labelpad=12)       2862
ax[2,0].text(1.06, 0.55, "0.8", rotation=0,              2863
             transform=ax[2,0].transAxes, color='red')      2864
ax[3,0].plot(fbmp1)                                    2865
ax[3,0].xaxis.set_visible(False)                         2866
ax[3,0].set_yticks([])                                  2867
ax[3,0].set_ylabel("0.1", rotation=0, labelpad=12)       2868
ax[3,0].text(1.06, 0.55, "1.2", rotation=0,              2869
             transform=ax[3,0].transAxes, color='red')      2870
ax[4,0].plot(fbmp5)                                    2871
ax[4,0].xaxis.set_visible(False)                         2872
ax[4,0].set_yticks([])                                  2873
ax[4,0].set_ylabel("0.5", rotation=0, labelpad=12)       2874
ax[4,0].text(1.08, 0.55, "2", rotation=0,                2875
             transform=ax[4,0].transAxes, color='red')      2876
ax[5,0].plot(fbmp9)                                    2877
ax[5,0].set_yticks([])                                  2878
ax[5,0].set_ylabel("0.9", rotation=0, labelpad=12)       2879

```

```

2899 ax[5,0].set_xlabel("Time")
2900
2901 ax[5,0].text(1.06, 0.55, "2.8", rotation=0,
2902         transform=ax[5,0].transAxes, color='red')
2903
2904
2905
2906 line = lines.Line2D([0.1, 1.05], [0.495, 0.495], transform=fig.transFigure, color='black',
2907 fig.add_artist(line)
2908
2909 fig.text(1, 0.705, r"$H=\frac{\beta+1}{2}$", ha='center', va='center', fontsize=18, transform=fig.transFigure)
2910 fig.text(1, 0.305, r"$H=\frac{\beta-1}{2}$", ha='center', va='center', fontsize=18, transform=fig.transFigure)
2911
2912
2913
2914 fig.text(0.11, .9, r"H", fontsize=14, ha='center', va='center', transform=fig.transFigure)
2915 fig.text(0.5, .9, r"$\beta$", fontsize=14, ha='center', va='center', transform=fig.transFigure)
2916
2917
2918
2919 freq,power,pred_power = psd(fgnp1)
2920
2921 ax[0,1].plot(freq,power)
2922 ax[0,1].set_title("Power Spectral Density")
2923
2924 ax[0,1].plot(freq[1:], pred_power, color='red')
2925
2926 ax[0,1].set_xscale('log')
2927 ax[0,1].set_yscale('log')
2928
2929 ax[0,1].xaxis.set_visible(False)
2930
2931 ax[0,1].yaxis.tick_right()
2932 ax[0,1].set_ylim(1e-4,10)
2933
2934
2935
2936 freq,power,pred_power = psd(fgnp5)
2937
2938 ax[1,1].plot(freq,power)
2939 ax[1,1].plot(freq[1:], pred_power, color='red')
2940
2941 ax[1,1].set_xscale('log')
2942 ax[1,1].set_yscale('log')
2943
2944

```

```

ax[1,1].xaxis.set_visible(False)                                2945
ax[1,1].yaxis.tick_right()                                    2946
ax[1,1].set_ylabel(r"$\log|A(f)|^2$")                         2947
ax[1,1].set_ylim(1e-5,1e-2)                                  2948
   2949
   2950
   2951
   2952
freq,power,pred_power = psd(fgnp9)                           2953
   2954
ax[2,1].plot(freq,power)                                     2955
   2956
ax[2,1].plot(freq[1:], pred_power, color='red')             2957
   2958
ax[2,1].set_xscale('log')                                    2959
   2960
ax[2,1].set_yscale('log')                                    2961
   2962
ax[2,1].xaxis.set_visible(False)                            2963
   2964
ax[2,1].yaxis.tick_right()                                2965
   2966
ax[2,1].set_ylim(1e-9,1e-2)                                2967
   2968
freq,power,pred_power = psd(fbmp1)                          2969
   2970
ax[3,1].plot(freq,power)                                     2971
   2972
ax[3,1].plot(freq[1:], pred_power, color='red')            2973
   2974
ax[3,1].set_xscale('log')                                    2975
   2976
ax[3,1].set_yscale('log')                                    2977
   2978
ax[3,1].xaxis.set_visible(False)                            2979
   2980
ax[3,1].yaxis.tick_right()                                2981
   2982
freq,power,pred_power = psd(fbmp5)                          2983
   2984
ax[4,1].plot(freq,power)                                     2985
   2986
ax[4,1].plot(freq[1:], pred_power, color='red')            2987
   2988
ax[4,1].set_xscale('log')                                    2989
   2990

```

```

2991 ax[4,1].xaxis.set_visible(False)
2992
2993 ax[4,1].set_ylabel(r"$|\log|A(f)|^2$")
2994 ax[4,1].yaxis.tick_right()
2995
2996 ax[4,1].set_ylim(1e-5,1e3)
2997
2998
2999 freq,power,pred_power = psd(fbmp9)
3000
3001 ax[5,1].plot(freq,power)
3002
3003 ax[5,1].plot(freq[1:], pred_power, color='red')
3004 ax[5,1].set_xscale('log')
3005
3006 ax[5,1].set_yscale('log')
3007
3008 #ax[5,1].set_xticklabels([])
3009 ax[5,1].yaxis.tick_right()
3010
3011 ax[5,1].set_xlabel("$\log(f)$")
3012
3013
3014 plt.savefig('../image/typicalsamplepaths.png', dpi=600, bbox_inches='tight', format='png')
3015
3016 plt.show()
3017
3018
3019
3020
3021
3022
3023
3024
3025
3026
3027
3028
3029
3030
3031
3032
3033
3034
3035
3036

```

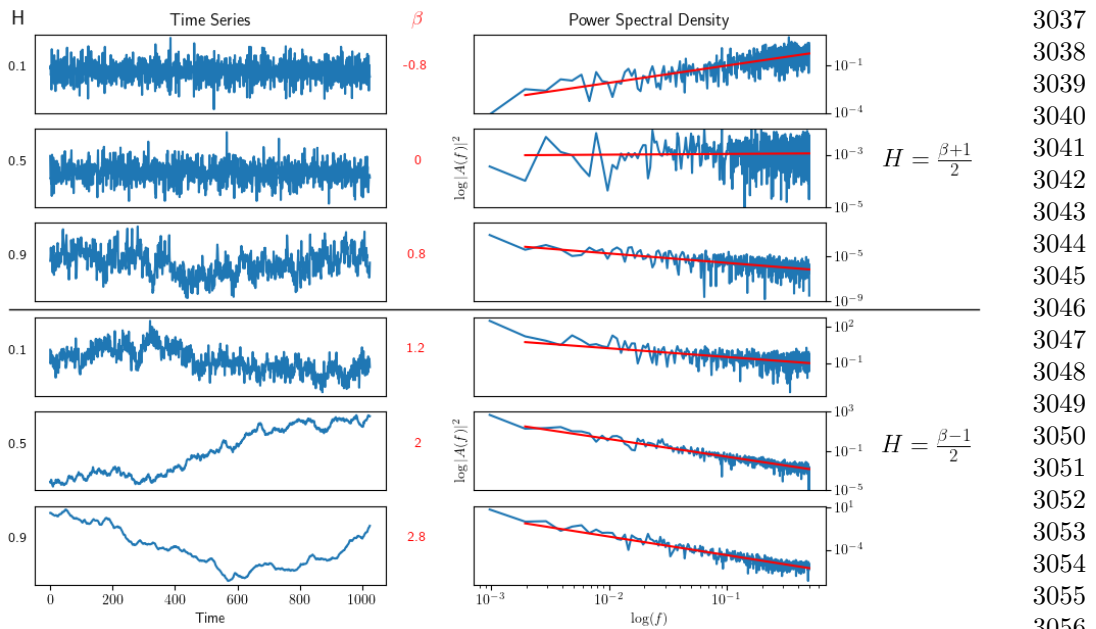


**Figure 7. Simulated fractional Gaussian noise and fractional Brownian motion.** Raw simulated time-series with 1,024 time-points and known Hurst values. Signals were created using the Davies-Harte method. a-c) are fractional Gaussian noise while d-f are fractional Brownian motion. a) and d) have H values of 0.1; b) and e) have H values of 0.5; and c) and f) have H values of 0.9. Note how fractional Gaussian noise remain centered around a mean (i.e. stationary), while fractional Brownian motion is free to wander (i.e. non-stationary). Exact fractal time-series were created using the Davies-Harte method.

⋮

⋮

If the class of signal is not appropriately identified — for example, when  $\beta$  is  $\sim 1$  — it is possible to seriously miscalculate the H value, such that a true  $H \sim 0.9$  will be calculated as 0.1. Therefore, algorithms and research in properly classifying fractal signals is crucially important.

3083 **Prerequisites to measuring H**

3084

3085 **Time-points**

3086

3087 Before determining if a time-series exhibits a power-law scaling relationship, one  
3088 should first determine if the time-series has enough time-points to do so. The rule  
3090 of thumb is that the power law relationship should be present in a range larger  
3092 than two decades in the frequency domain of a PSD [24]. Due to the Whittaker–  
3093 Nyquist-Shannon sampling theorem [25], one requires two times as many time-points  
3095 as frequency samples. Since two decades in the frequency domain is 100 distinct  
3097 frequencies, one would required at least 200 time-points to proceed.  
3098

3099

3100 **Power-law scaling relationship**

3101

3102 The next step would be to perform a periodogram or PSD and test for a power-law  
3103 scaling relationship. Usually power laws are tested using a probability distribution  
3105 [26]. However, as the PSD is not a probability distribution, alternative methods must  
3107 be used. A goodness-of-fit test can be devised based on Clauset et al. [26], which can  
3108 also help us derive the SR (i.e.  $freq_{min}$  and  $freq_{max}$ ). First, a PSD is produced, and  
3110 the variance ( $\sigma^2$ ),  $\beta$ , and H are computed using Equation 8. Next, the Kolmogorov–  
3112 Smirnov statistic [27, 28] is used to measure the distance D between the raw PSD data-  
3113 points and the best-fit linear-regression line used to calculate H (i.e. the residuals).  
3114 The D in this case is the largest residual error. Then, 1,000 time series of either fGn  
3116 or fBm (depending on what value of  $\beta$  was found; see Equation 8) with the same  
3118 length ( $n > 200$ ),  $\sigma^2$ , and Hurst exponent are generated using one of several methods  
3120 for producing exact fractal signals: spectral synthesis method (SSM) [29], Davies–  
3122 Harte method (DH) [30], Cholesky method [31], or the Hosking’s method [32]. Each  
3123 synthetic time-series is converted to a PSD, and the Kolmogorov–Smirnov statistic  
3125 is used to measure the distance D between the raw PSD data-points and the best-fit  
3127 linear-regression line. The  $p$ -value is defined as the fraction of synthetic time series  
3128

with Ds that are larger than the original D of the original time-series. The larger the	3129
<i>p</i> -value, the more plausible the synthetic model (either fGn or fBm) is for representing	3130
the original time-series, and the better the fit of the original data to a scale-free	3131
distribution. The null-hypothesis that the time-series is not scale free is rejected if <i>p</i>	3132
< 0.05 (i.e. if <i>p</i> > 0.05, we say that the time-series is scale-free).	3133
	3134
	3135
	3136
	3137
However, this method can be computationally intensive, and prone to false negatives,	3138
especially signals with very high or low H values. One solution is, instead of applying	3139
this test to every voxel in a 4D fMRI brain scan, to segment the brain into separate	3140
ROIs (e.g. anatomically based on an atlas, or functionally by first running ICA to	3141
identify RSNs), average the time-series within each ROI, which will improve SNR,	3142
and then run the power-law scaling test.	3143
	3144
	3145
	3146
	3147
	3148
A sample python code is provide in Section 2	3149
	3150
<b>Scaling range</b>	3151
<b>fGn or fBm</b>	3152
<b>Choosing the right method</b>	3153
Ideally therefore, a long memory process signal should be categorized as either stationary	3154
(fGn) or non-stationary (fBm) and the variance and correlation defined. from [24]	3155
	3156
	3157
	3158
	3159
	3160
	3161
	3162
<b>Methods of measuring H</b>	3163
Fractal methods are diverse, but their approaches have one thing in common in that	3164
they employ equation (2) in fitting their proposed model to data pairs of log feature	3165
versus log scale for finding the scaling exponent, , from the regression slope. Each fractal	3166
analysis tool has different performance, prerequisite conditions, and limitations, and each	3167
needs thorough evaluation in order to avoid bias or misinterpretation of the derived fractal	3168
	3169
	3170
	3171
	3172
	3173
	3174

3175 parameters [5, 6, 8, 9], especially when applied to physiological signals which may be  
3176 contaminated with noise [15, 28]. from [24]  
3177

3178

3179

## 3180 **Neuroscience Applications**

3181

3182 H has emerged as a valuable tool in neuroscience and clinical research. Typically, H  
3183 values reported in adult brains are above 0.5, with higher H values in grey matter  
3184 than white matter or cerebrospinal fluid [33, 34]. Some key findings from neuroscience  
3185 research include: a decrease in H during task performance [35, 36]; negative corre-  
3186 lations with task novelty and difficulty [37]; increases with age in the frontal and  
3187 parietal lobes [33], and hippocampus [38]; decreases with age in the insula, and lim-  
3188 3190 bic, occipital and temporal lobes [33]; H < 0.5 in preterm infants [39]; and more [40].  
3191

3192 In terms of clinical findings, abnormal H values have been identified in Alzheimer's  
3193 disease (AD) [41, 42], autism spectrum disorder (ASD) [43–46], mild traumatic brain  
3194 3196 injury [47], major depressive disorder [48, 49] and schizophrenia [46, 50].  
3197

3198

3199

## 3200 **fMRI preprocessing considerations**

3201

### 3202 **Nuissance regression**

3203

3204 When attempting to regress out non-BOLD signal, it is important to apply the regres-  
3205 sion at the same time, and not in succession. Even performing a band-pass filter after  
3206 3207 nuissance regression can re-introduce noise components [51].  
3208

3209

### 3210 **Detrending**

3211

3212 see Tanabe et al. [52]

3213

3214

3215

3216

3217

3218

3219

3220

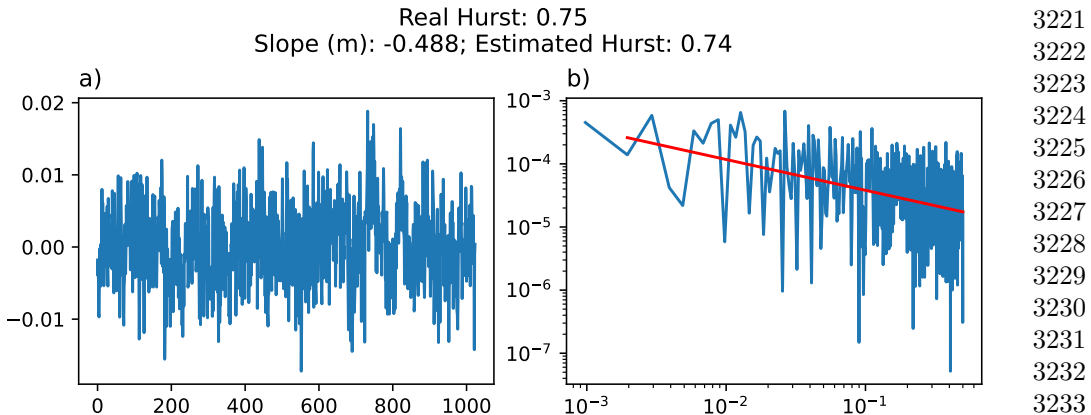


**Figure 8. Simulated fractional Gaussian noise.** a) Raw simulated time-series with 1,024 time-points and a known Hurst value of 0.75; b) The same signal from a) in a log-log power spectral density plot and a linear-regression used to calculate the estimated Hurst value.

## Hurst Reviews

Nonparametric trend estimation in the presence of fractal noise:

Application to fMRI time-series analysis - Afshinpour et al. (2008)

[53]

In this paper, a method for estimating trend in the presence of fractal noise is proposed and applied to fMRI time-series. To this end, a partly linear model (PLM) is fitted to each time-series. The parametric and nonparametric parts of PLM are considered as contributions of hemodynamic response and trend, respectively. Using the whitening property of wavelet transform, the unknown components of the model are estimated in the wavelet domain. The results of the proposed method are compared to those of other parametric trend-removal approaches such as spline and polynomial models. It is shown that the proposed method improves activation detection and decreases variance of the estimated parameters relative to the other methods.

Notes:

3267 • trend estimation paper

3268 • 1.5T, 3.9x3.9x6mm, 1.648s TR, 256 time-points  
3269

3270 • Hurst method: Wavelet db4 with 5 scales

3271

3272

## 3273 Fractal Analysis of BOLD time-series in a Network Associated With 3274

3275 Waiting Impulsivity - Akhrif et al. (2018) [54]

3276

examined **103** healthy male students at **rest** and while performing the 5-choice serial reaction time **task**. We addressed fractality in a network associated with waiting impulsivity using the **adaptive fractal analysis (AFA)** approach to determine H. We revealed the fractal nature of the impulsivity network. Furthermore, fractality was influenced by individual impulsivity in terms of decreasing fractality (H) with higher impulsivity in regions of top-down control (left middle frontal gyrus) as well as reward processing (nucleus accumbens and anterior cingulate cortex).

3281  
2009

3288

3289 Notes:  
3200

3290

3291

- fMRI split into low and high frequency components. LFC is the second order polynomial that is a smooth and global fit of the original time course.

• AFA: variance of fluctuation computed around, in this case, a second order polynomial trend  $v(i)$  fitted to time-series within each segment  $w$ , and its size:

3299

$$F(w) = \sqrt{\frac{1}{N} \sum_{i=1}^N (u(i) - v(i))^2} \sim w^H \quad (10)$$

3303

3304 N: length of the time-series

3305

3306

$$w = 2n + 1, n = 5, 6, \dots, 13$$

3309  
2210

3310  
2211

3311

3312

```

Example code:                                3313
  3314
import numpy as np                         3315
  3316
  3317
def adaptive_fractal_analysis(signal, n_values=range(5, 14)): 3318
    """  3319
  3320
  3321
  3322
  3323
  3324
  3325
  3326
  3327
  3328 as w = 2n + 1.
  3329
  3330
  3331
  3332
  3333
  3334
  3335
  3336
  3337
  3338
  3339
  3340
  3341
  3342
  3343
  3344
  3345
  3346
  3347
  3348
  3349
  3350
  3351
  3352
  3353
  3354
  3355
  3356
  3357
  3358

    Perform Adaptive Fractal Analysis (AFA) to compute the Hurst exponent.

Parameters:
    signal (array-like): time-series data to analyze.
    n_values (iterable): Sequence of `n` values to define window sizes
    Returns:
        float: Estimated Hurst exponent (H).
    """
# Define window sizes as w = 2n + 1
window_sizes = [2 * n + 1 for n in n_values]
fluctuations = []

for window_size in window_sizes:
    segment_variances = []
    for start in range(0, len(signal) - window_size + 1, window_size):
        # Extract the window
        window = signal[start:start + window_size]
        # Fit a second-order polynomial (quadratic fit) and compute residual
        x = np.arange(len(window))
        p = np.polyfit(x, window, deg=2) # Degree 2 polynomial
        residual = window - np.polyval(p, x)

```

```

3359         # Compute variance of the residuals
3360         variance = np.var(residual)
3361         segment_variances.append(variance)
3362
3363
3364
3365
3366         # Compute average variance for this window size
3367         fluctuations.append(np.mean(segment_variances))
3368
3369
3370
3371         # Fit the scaling law: log(fluctuations) vs. log(window_sizes)
3372         log_window_sizes = np.log(window_sizes)
3373         log_fluctuations = np.log(fluctuations)
3374
3375         slope, intercept = np.polyfit(log_window_sizes, log_fluctuations, deg=1)
3376
3377
3378
3379         # The slope corresponds to the Hurst exponent
3380
3381     return slope
3382
3383
3384 Endogenous human brain dynamics recover slowly following
3385
3386 cognitive effort - Barnes et al. (2009) [55]
3387
3388 1) Does performance of a cognitively effortful task significantly change fractal
3389 scaling properties of fMRI time-series compared to their values before task per-
3390 formance? 2) If so, can we relate the extent of task-related perturbation to the
3391 difficulty of the task? This result supports the model that endogenous low fre-
3392 quency oscillatory dynamics are relevant to the brain's response to exogenous
3393 stimulation. Moreover, it suggests that large-scale neurocognitive systems mea-
3394 sured using fMRI, like the heart and other physiological systems subjected to
3395 external demands for enhanced performance, can take a considerable period of
3396 time to return to a stable baseline state.
3397
3398
3399
3400
3401
3402
3403
3404

```

<b>Notes:</b>	3405
	3406
	3407
• maximum likelihood in the wavelet domain	3408
	3409
	3410
<b>Wavelets and functional magnetic resonance imaging of the human brain - Bullmore et al. (2004) [56]</b>	3411
	3412
	3413
	3414
We provide a brief formal introduction to key properties of the DWT and review the growing literature on its application to fMRI. We focus on three applications in particular: (i) wavelet coefficient resampling or “wavestrapping” of 1-D time-series, 2- to 3-D spatial maps and 4-D spatiotemporal processes; (ii) wavelet-based estimators for signal and noise parameters of time-series regression models assuming the errors are fractional Gaussian noise (fGn); and (iii) wavelet shrinkage in frequentist and Bayesian frameworks to support multiresolution hypothesis testing on spatially extended statistic maps.	3415
	3416
	3417
	3418
	3419
	3420
	3421
	3422
	3423
	3424
	3425
	3426
<b>Notes:</b>	3427
	3428
	3429
• This paper suggests that motion correction translates many fBm signals to fGn... however, it is not clear where this data comes from.	3430
	3431
	3432
	3433
	3434
<b>Fractal-Based Analysis of fMRI BOLD Signal During Naturalistic Viewing Conditions - Campbell et al. (2021) [57]</b>	3435
	3436
	3437
	3438
We performed fractal analysis on Human Connectome Project 7T fMRI data ( $n = 72$ , 41 females, mean age $29.46 \pm 3.76$ years) to compare H across movie-watching and rest. Results: In contrast to previous work using conventional tasks, we found higher H values for movie relative to rest (mean difference = 0.014; $p = 5.279 \times 10^{-7}$ ; 95% CI [0.009, 0.019]). H was significantly higher in movie than rest in the visual, somatomotor and dorsal attention networks, but was significantly lower during movie in the frontoparietal and default networks. We found no cross-condition differences in test-retest reliability of	3439
	3440
	3441
	3442
	3443
	3444
	3445
	3446
	3447
	3448
	3449
	3450

3451 H. Finally, we found that H of movie-derived stimulus properties (e.g., luminance changes)  
3452 were fractal whereas H of head motion estimates were non-fractal.  
3453

3454  
3455 **Notes:**  
3456

3457  
3458 •  
3459  
3460

3461 **Scale-free brain dynamics under physical and psychological distress:**  
3462

3463 **Pre-treatment effects in women diagnosed with breast cancer -**  
3464

3465 **Churchill et al. (2015) [58]**  
3466

3467 In a BOLD functional magnetic resonance imaging study, we scanned three groups during a  
3468 working memory task: women scheduled to receive chemotherapy or radiotherapy and aged-  
3469 matched controls. Surprisingly, patients' BOLD signal exhibited greater H with increasing  
3470 intensity of anticipated treatment. However, an analysis of H and functional connectivity  
3471 against self-reported measures of psychological distress (Worry, Anxiety, Depression) and  
3472 physical distress (Fatigue, Sleep problems) revealed significant interactions. The modula-  
3473 tion of (Worry, Anxiety) versus (Fatigue, Sleep Problems, Depression) showed the strongest  
3474 effect, where higher worry and lower fatigue was related to reduced H in regions involved  
3475 in visuospatial search, attention, and memory processing. This is also linked to decreased  
3476 functional connectivity in these brain regions.  
3477

3478  
3479  
3480 **Notes:**  
3481

3482  
3483  
3484 **The suppression of scale-free fMRI brain dynamics across three**  
3485 **different sources of effort: Aging, task novelty and task difficulty -**  
3486

3487 **Churchill et al. (2016) [37]**  
3488

3489 Decreases in the Hurst exponent (H), which quantifies scale-free signal, was related to three  
3490 different sources of cognitive effort/task engagement: 1) task difficulty, 2) task novelty,  
3491 and 3) aging effects. These results were consistently observed across multiple datasets  
3492

and task paradigms. We also demonstrated that estimates of H are robust across a range of time-window sizes. H was also compared to alternative metrics of BOLD variability (SDBOLD) and global connectivity (Gconn), with effort-related decreases in H producing similar decreases in SDBOLD and Gconn.

**Notes:**

**Interplay between functional connectivity and scale-free dynamics in intrinsic fMRI networks - Ciuciu et al. (2014) [35]**

We applied this framework to fMRI data acquired from healthy young adults at rest and performing a visual detection task. First, we found that scale-invariance existed beyond univariate dynamics, being present also in bivariate cross-temporal dynamics. Second, we observed that frequencies within the scale-free range do not contribute evenly to interregional connectivity, with a systematically stronger contribution of the lowest frequencies, both at rest and during task. Third, in addition to a decrease of the Hurst exponent and inter-regional correlations, task performance modified cross-temporal dynamics, inducing a larger contribution of the highest frequencies within the scale-free range to global correlation. Lastly, we found that across individuals, a weaker task modulation of the frequency contribution to inter-regional connectivity was associated with better task performance manifesting as shorter and less variable reaction times. These findings bring together two related fields that have hitherto been studied separately – resting-state networks and scale-free dynamics, and show that scale-free dynamics of human brain activity manifest in cross-regional interactions as well.

**Notes:**

3543 **Temporal fractal analysis of the rs-BOLD signal identifies brain**  
3544  
3545 **abnormalities in autism spectrum disorder - Dona et al. (2017) [43]**  
3546  
3547 "It is important to mention here that fractal dimension estimation based on adisper-  
3548 sional analysis is quite robust with respect to uncorrelated noise and does not require  
3549 preprocessing"  
3550  
3551  
3552  
3553 **Notes:**  
3554  
3555  
3556 • ASD = reduced FD = increased H;  
3557 • rare study to properly define fGn vs fBm first?  
3559  
3560  
3561 **Fractal analysis of brain blood oxygenation level dependent (BOLD)**  
3562 **signals from children with mild traumatic brain injury (mTBI) -**  
3563  
3564 **Dona et al. (2017) [47]**  
3565  
3566 **Notes:**  
3567  
3568  
3569 • children with mTBI; mTBI = reduced FD = increased H  
3570  
3571 • rare study to properly define fGn vs fBm first?  
3572  
3573  
3574 **Hurst Exponent Analysis of Resting-State fMRI Signal Complexity**  
3575  
3576 **across the Adult Lifespan - Dong et al. (2018) [33]**  
3577  
3578 Region-wise and voxel-wise analyses were performed to investigate the effects of age, gen-  
3579 der, and their interaction on complexity. In region-wise analysis, we found that the healthy  
3580 aging is accompanied by a loss of complexity in frontal and parietal lobe and increased  
3581 complexity in insula, limbic, and temporal lobe. Meanwhile, differences in HE between gen-  
3582 ders were found to be significant in parietal lobe ( $p = 0.04$ , corrected). However, there was  
3583 no interaction between gender and age. In voxel-wise analysis, the significant complexity  
3584 decrease with aging was found in frontal and parietal lobe, and complexity increase was  
3585  
3586  
3587  
3588

found in insula, limbic lobe, occipital lobe, and temporal lobe with aging. Meanwhile, differences in HE between genders were found to be significant in frontal, parietal, and limbic lobe. Furthermore, we found age and sex interaction in right parahippocampal gyrus ( $p = 0.04$ , corrected). Our findings reveal HE variations of the rs-fMRI signal across the human adult lifespan and show that HE may serve as a new parameter to assess healthy aging process. 3589  
3590  
3591  
3592  
3593  
3594  
3595  
3596  
3597  
3598  
3599  
3600  
3601  
3602  
3603  
3604  
3605  
3606  
3607  
3608  
3609  
3610  
3611  
3612  
3613  
3614  
3615  
3616  
3617  
3618  
3619  
3620  
3621  
3622  
3623  
3624  
3625  
3626  
3627  
3628  
3629  
3630  
3631  
3632  
3633  
3634

**Notes:**

- They state that increase in age = decrease in complexity

**Pitfalls in fractal time-series analysis: fMRI BOLD as an exemplary case - Eke et al. (2012) [59]**

**Wavelet-Generalized Least Squares: A New BLU Estimator of Linear Regression Models with 1/f Errors - Fadili & Bullmore (2002) [60]**

**Not in one metric: Neuroticism modulates different resting state metrics within distinctive brain regions - Gentili et al. (2017) [61]**

Metrics more related to the measurement of regional intrinsic brain activity (fALFF, ALFF and REHO), or that provide a parsimonious index of integrated and segregated brain activity (HE), were more broadly modulated in regions related to emotions and their regulation. Metrics related to connectivity were modulated across a wider network of areas. Overall, these results show that neuroticism affects distinct aspects of brain resting state activity.

3635 **Notes:**

3636

3637

3638 • “parsimonious index of integrated and segregated brain activity (HE)”

3639

3640 • HE was inversely correlated to neuroticism

3641

3642

3643 **Proneness to social anxiety modulates neural complexity in the**

3644

3645 **absence of exposure: A resting state fMRI study using Hurst**

3646

3647 **exponent - Gentili et al. (2015) [62]**

3648

3649 Results from fALFF were highly consistent with those obtained using LSAS and BFNE  
3650 to predict HE. Overall our data indicate that spontaneous brain activity is influenced by  
3651 the degree of social anxiety, on a continuum and in the absence of social stimuli. These  
3652 findings suggest that social anxiety is a trait characteristic that shapes brain activity and  
3653 predisposes to different reactions in social contexts.

3654

3655

3656 **Notes:**

3657

3658

3659

3660 • “A recent article (Rubin et al., 2013) analyzes the robustness of different algorithms

3661

3662 with respect to possible fMRI artifacts and time-series lengths. In particular, the  
3663 relevance of preprocessing steps as motion correction, detrending and filtering were  
3664 evaluated both on simulated and real fMRI data, while other preprocessing steps  
3665 like segmentation were not evaluated, although they may have an impact on”

3666

3667 • “The HE of fMRI time-series is generally higher in gray matter than in white matter  
3668 (Maxim et al., 2005), augments in the hippocampus with aging, and decreases with  
3669 cholinergic transmission enhancement (Wink et al., 2006)”

3670

3671 • “As pointed out by Maxim (Maxim et al., 2005), fMRI noise, after these pre-  
3672 processing steps, can be described as fGn.”

3673

3674

3675

3676

3677

3678

3679

3680

• “The HE of fMRI time-series is generally higher in gray matter than in white matter (Maxim et al., 2005), augments in the hippocampus with aging, and decreases with cholinergic transmission enhancement (Wink et al., 2006).”	3681 3682 3683 3684 3685 3686 3687 3688 3689 3690 3691 3692 3693 3694 3695 3696 3697 3698 3699 3700 3701 3702 3703 3704 3705 3706 3707 3708 3709 3710 3711 3712 3713 3714 3715 3716 3717 3718 3719 3720 3721 3722 3723 3724 3725 3726
<b>Real-time fractal signal processing in the time domain. - Hartmann et al. (2013) [63]</b>	3697 3698 3699 3700 3701 3702 3703 3704 3705 3706 3707 3708 3709 3710 3711 3712 3713 3714 3715 3716 3717 3718 3719 3720 3721 3722 3723 3724 3725 3726
Here we introduce real-time variants of the Detrended Fluctuation Analysis (DFA) and the closely related Signal Summation Conversion (SSC) methods, which are suitable to estimate the fractal exponent in one pass.	3701 3702 3703 3704 3705 3706 3707 3708 3709 3710 3711 3712 3713 3714 3715 3716 3717 3718 3719 3720 3721 3722 3723 3724 3725 3726
<b>Altered fractal dynamics of gait: Reduced stride-interval correlations with aging and Huntington’s disease. - Hausdoff et al. (1997) [64]</b>	3707 3708 3709 3710 3711 3712 3713 3714 3715 3716 3717 3718 3719 3720 3721 3722 3723 3724 3725 3726
<b>Notes:</b>	3711 3712 3713 3714 3715 3716 3717 3718 3719 3720 3721 3722 3723 3724 3725 3726
• Gait... not fMRI	3714 3715 3716 3717 3718 3719 3720 3721 3722 3723 3724 3725 3726
<b>Scale-Free Properties of the Functional Magnetic Resonance Imaging Signal during Rest and Task - He (2011) [36]</b>	3717 3718 3719 3720 3721 3722 3723 3724 3725 3726
its power-law exponent differentiates between brain networks and correlates with fMRI signal variance and brain glucose metabolism. Importantly, in parallel to brain electrical field potentials, the variance and power-law exponent of the fMRI signal decrease during	3721 3722 3723 3724 3725 3726

task activation, suggesting that the signal contains more long-range memory during rest and conversely is more efficient at online information processing during task. The scale-free properties of the fMRI signal and brain electrical field potentials bespeak their respective stationarity and nonstationarity. This suggests that neurovascular coupling mechanism is likely to contain a transformation from nonstationarity to stationarity.

The fMRI signal time course from each ROI was extracted for each subject and fMRI run. The normalized or non-normalized power spectrum of the fMRI signal was computed using the Bartlett smoothing procedure of deriving the power spectral function from the lagged autocorrelation or auto-covariance function, respectively (Jenkins and Watts, 1998). A Tukey window of 20 fMRI frame width was applied for additional smoothing. The power spectra were then averaged across runs and subjects and across homologous ROIs, resulting in an average power spectrum for each of 21 brain regions (Fig. 2A). Finally, to obtain the power-law exponent , the <0.1 Hz range of each average power spectrum was fit with a power-law function:  $P(f) \sim 1/f$  using a least-squares fit. Using the low-frequency range to fit the power-law exponent avoids aliasing artifact in higher-frequency range (we used TR of 2.16 s, hence Nyquist limit is 0.23 Hz) and yields reliable measurement of the scale-free distribution (Eke et al., 2002).

The DFA method has the particular advantage of being applicable to both stationary and nonstationary data. To analyze our fMRI data, window lengths of 5, 10, 19, 38, and 95 fMRI frames were chosen so that the number of frames in each run (190 after discarding the first four frames) is an integer multiple of the window length.

<b>Fractal characterization of complexity in dynamic signals:</b>	3773
Application to cerebral hemodynamics - Herman (2009) [12]	3774
	3775
	3776
<b>Identification of brain activity from fMRI data: Comparison of three fractal scaling analyses. - Hu (2006) [65]</b>	3777
	3778
	3779
	3780
<b>A shift to randomness of brain oscillations in people with autism.</b>	3781
Lai (2010) [44]	3782
	3783
	3784
Complex fractal scaling of fMRI time-series was found in both groups but globally there was a significant shift to randomness in the ASC (mean $H = .758$ , $SD = .045$ ) compared with neurotypical volunteers (mean $H = .788$ , $SD = .047$ ).	3785
	3786
	3787
	3788
	3789
	3790
<b>Extraversion is encoded by scale-free dynamics of default mode network. Lei (2013) [66]</b>	3791
	3792
	3793
	3794
<b>Fractional Gaussian noise, functional MRI and Alzheimer's disease.</b>	3795
Maxim (2005) [41]	3796
	3797
	3798
we adopted the Davies-Harte algorithm, which is both exact and fast, to generate the fGn simulations used here. For each value of $H = 0.1, \dots, 0.9$ , we simulated 1000 realizations of fGn with 512 time-points in each series; we set $\omega^2 = 1$ for all simulations.	3799
	3800
	3801
	3802
	3803
	3804
<b>NOTES:</b>	3805
	3806
	3807
• This paper has the figure showing signal goes from fBm to fGn with proper motion regression	3808
	3809
	3810
	3811
	3812
<b>Decomposing multifractal crossovers. Nagy (2017) [67]</b>	3813
The NIRS and fMRI-BOLD low-frequency fluctuations were dominated by a multifractal component over an underlying biologically relevant random noise, thus forming a bimodal	3814
	3815
	3816
	3817
	3818

3819 signal. The crossover between the EEG signal components was found at the boundary  
3820 between the and bands, suggesting an independent generator for the multifractal  
3821 rhythm. The robust implementation of the SFD method should be regarded as essential  
3822 in the seamless processing of large volumes of bimodal fMRI-BOLD imaging data for the  
3823 topology of multifractal metrics free of the masking effect of the underlying random noise.  
3824  
3825  
3826  
3827

3828 **Optimizing complexity measures for fMRI data: Algorithm,**

3829

3830 **artifact, and sensitivity. Rubin (2013) [68]**

3831

3832 Power-spectrum, Higuchi's fractal dimension, and generalized Hurst exponent based esti-  
3833 mates were most successful by all criteria; the poorest-performing measures were wavelet,  
3834 detrended fluctuation analysis, aggregated variance, and rescaled range. Our results clearly  
3835 demonstrate that decisions regarding choice of algorithm, signal processing, time-series  
3836 length, and scanner have a significant impact on the reliability and sensitivity of com-  
3837 plexity estimates. operating on the edge of chaos, complex systems position themselves  
3838 for optimal responsivity to inputs, as well as ability to maintain homeostatic regulation.  
3839 Daubechies wavelet based computations (Hdb) *have long computation times, are not sen-*  
3840 *sitive to spikes, and show poor sensitivity to activation, tissue type, and emotional content;*  
3841 *for these Daubechies wavelet based estimates the overall performance increases with the*  
3842 *wavelet order up to a point (Hdb8), and then deteriorates. HRS and HAV, performed poorly*  
3843 *across the board. In terms of image contrast, overlap with activation, and group differences,*  
3844 *HDFA performed poorly as well, with HDFA-S outperforming HDFA and HDFA-L, sug-*  
3845 *gesting that the bulk of useful information is found at shorter lags. The most consistently*  
3846 *successful measures were the powerspectrum based measures HFFT and HpWelch, with*  
3847 *the latter slightly outperforming the former while taking much longer to compute Second,*  
3848 *it appears that detrending, regressing out the global mean, and excluding low frequencies*  
3849 *improves agreement between complexity and activation. 300-600 time-points Finally, the*  
3850 *best measures to use are either the power-spectrum based ones (HFFT or HpWelch) on a*  
3851 *restricted frequency range (above ,0.01 Hz),*

3852

3853

3854

3855

3856

3857

3858

3859

3860

3861

3862

3863

3864

**Mutual information identifies spurious Hurst phenomena in resting state EEG and fMRI data. von Wegner (2018) [69]**

In these processes, which do not have long-range memory by construction, a spurious Hurst phenomenon occurs due to slow relaxation times and heteroscedasticity (time-varying conditional variance). In summary, we find that mutual information correctly distinguishes long-range from short-range dependence in the theoretical and experimental cases discussed. Our results also suggest that the stationary fGn process is not sufficient to describe neural data, which seem to belong to a more general class of stochastic processes, in which multiscale variance effects produce Hurst phenomena without long-range dependence. In our experimental data, the Hurst phenomenon and long-range memory appear as different system properties that should be estimated and interpreted independently.

3911 **References**

3912

3913

3914

3915

3916

3917

3918

3919

3920

3921

3922

3923

3924

3925

3926

3927

3928

3929

3930

3931

3932

3933

3934

3935

3936

3937

3938

3939

3940

3941

3942

3943

3944

3945

3946

3947

3948

3949

3950

3951

3952

3953

3954

3955

3956

<b>Appendix</b>	3957
	3958
<b>Python code</b>	3959
	3960
	3961
<b>Sample python code for testing power-law scaling</b>	3962
	3963
<b>print("HELLO")</b>	3964
	3965
	3966
	3967
	3968
	3969
	3970
	3971
	3972
	3973
	3974
	3975
	3976
	3977
	3978
	3979
	3980
	3981
	3982
	3983
	3984
	3985
	3986
	3987
	3988
	3989
	3990
	3991
	3992
	3993
	3994
	3995
	3996
	3997
	3998
	3999
	4000
	4001
	4002